Optoelectronic Tweezers Meet Microfluidics: A Powerful Approach for Micromanipulation and Biochemical Analysis

Zonghao Li[1,2], Chunbo Yao[1,2], Gong Li[1], Henan Du[1], Hang Li[2,3,4]*, Wei-Hua Yu[1,2]*, Rongxin Fu[2,3,4], Kangfu Chen[1,2], Meiyi Zhou[1,2], Huikai Xie[1,2], Wei Xie[5], Hainan Xie[5], Lingling Shui[6], Mohammad Asif Zaman[7], Lambertus Hesselink[7], Steven L. Neale[8], and Shuailong Zhang[1,2,3]*

[1] State Key Laboratory of Chips and Systems for Advanced Light Field Display, School of Integrated Circuits and Electronics, Beijing Institute of Technology, Beijing, 100081, China

[2] Engineering Research Center of Integrated Acousto-opto-electronic Microsystems (Ministry of Education of China), Chongqing Institute of Microelectronics and Microsystems, Beijing Institute of Technology, Chongqing, 400000, China

[3] Zhengzhou Research Institute, Beijing Institute of Technology, Zhengzhou, 450000, China

[4] School of Medical Technology, Beijing Institute of Technology, Beijing, 100081, China

[5] Optoseeker Biotechnology (Shenzhen) Co., Ltd., Shenzhen 518055, China

[6] School of Optoelectronic Science and Engineering, South China Normal University, Guangzhou 510006, China

[7] Department of Electrical Engineering, Stanford University, Stanford, California 94305, USA

[8] James Watt School of Engineering, University of Glasgow, Glasgow, G12 8QQ, United Kingdom

Author to whom correspondence should be addressed:

hang.li@bit.edu.cn

ywhbit@bit.edu.cn

shuailong.zhang@bit.edu.cn

Key Words:

Optoelectronic Tweezers; Microfluidics; Optical manipulation; Optoelectrowetting; Biochemical analysis; Optofluidics;

Abstract:

Optoelectronic tweezers (OET) have emerged as a transformative micromanipulation technology that transcends the limitations of traditional optical tweezers by utilizing light-induced dielectrophoresis. By leveraging the photoconductive effect of semiconductor materials, OET creates dynamic "virtual electrodes" that generate non-uniform electric fields, enabling high-throughput, non-invasive manipulation of micro- and nanoscale objects at optical power densities several orders of magnitude lower than conventional laser-based trapping. This review provides a rigorous examination of the fundamental physical principles of OET, while detailing its strategic integration with diverse microfluidic architectures. We systematically evaluate the synergy between OET and three primary fluidic platforms: channel microfluidics, which facilitates continuous-flow sorting and single-cell analysis; digital microfluidics (DMF), enabling precise particle handling within discrete droplets; and optoelectrowetting (OEW), which supports flexible droplet transport across complex topographies. Beyond laboratory research, we highlight the commercialization of these systems in biopharmaceutical discovery and the burgeoning role of Artificial Intelligence (AI) in catalyzing a paradigm shift toward autonomous, intelligent robotic platforms for precision medicine. Finally, we outline future frontiers in novel photoconductive materials and discuss the roadmap for highly integrated optofluidic systems in clinical diagnostics and cell therapy manufacturing.

I. Introduction

Micromanipulation is a technology that enables the precise localization, manipulation, and assembly of minute objects at the micron or nano scales. It facilitates the interaction of biological, chemical and material entities at the micro-scale. Existing micromanipulation methods are classified based on physical principles, and primarily include optical[1-3], acoustic[4-7], electrical[8-11], magnetic[12-14], and microfluidic manipulation[15,16]. In particular, optical

manipulation techniques show advantages due to their non-invasiveness, high spatial resolution, and compatibility with complex biological microenvironments. The first optical micromanipulation technique was developed by Arthur Ashkin and is referred to as optical tweezers (OT). OTs utilized high-intensity focused laser beams to capture and manipulate micro-particles or biomolecules through the optical gradient forces[1,2,17]. OTs have been successfully used to non-destructively manipulate bacteria and it is now a widely used tool in bioscience[18]. However, the high optical power required by OTs and create photothermal damage which limits its application for sensitive biosamples[19]. Also, the diffraction limited resolution of single laser OTs makes it difficult to manipulate nano-scale samples. To address some of the limitations of OTs, other optical manipulation techniques have been developed, including optoelectronic tweezers (OET)[20,21], plasmonic tweezers[22], photothermal tweezers[23-31], photoacoustic tweezers[32] and iontophoretic tweezers[33-35].

OET, developed in 2005 by Ming C. Wu and his then team members Pei Yu Chiou, Aaron T. Ohta[3], has demonstrated unparalleled excellence in high-throughput particle manipulation and assembly with much lower optical power than OTs. By projecting a spatially programmable light pattern onto a photoconductive substrate, OET forms localized high conductive region, referred to as light-induced virtual electrodes. When an alternating current (AC) field is applied between the photoconductive surface and a reference electrode, these virtual electrodes generate non-uniform electric field in the surrounding suspension medium, which interacts with particles or cells to exert electrokinetic forces, enabling non-contact, precise manipulation with minimized mechanical or chemical influence on the samples. Additionally, OET can generate large manipulation forces (nanonewtons) when sufficient AC voltage is applied. Most importantly, this force magnitude is almost independent of the optical power which only needs to excite the photoconductor and not do any mechanical work. Hence, the optical power can be as small as $1W/cm^{2,}$ which is several orders of magnitude lower than what is required for optical tweezers. OET also does not require the light source to be monochromatic or coherent. It has been demonstrated that relatively low powered broad band LEDs can be used as light source of OETs. A key advantage of OET over other optical manipulation techniques is parallelizability. A single light source can

be split into multiple sub patterns using a DMD and projected on an OET substrate to create multiple virtual electrodes. Each such virtual electrode can be separately controlled to create individual trap sites. Thus, parallel trapping and manipulation are easily achieved by programming the DMD. The optical sub-patterns only need to excite the photoconductor to create the local high-conductive region. The main manipulation force originates from the AC field. Hence, the optical power of single light source is sufficient to create a large number of independent virtual electrodes to achieve parallelization. Therefore, OET is easy-to-use and well-suited for dynamic control of biological samples with minimal sample damage. As such, OETs have been successfully used in various applications spanning physics, chemistry and biotechnology[36-38].

Although OET has shown strong capability in manipulating particles, its compatibility with microfluidic systems and fluidic environments remains challenging. In the past decades, researchers have dedicated to integrate OET with various microfluidic platforms, such as channel microfluidics, DMF, and OEW microfluidics[39-41]. OET-channel microfluidics integration increased the throughput and flexibility of particle manipulations through fluidic structures, being optimal for real-time sorting and assembly in continuous flow systems[42-44]. However, challenges exist in maintaining optical field stability, achieving high spatial resolution in microenvironments[45]. Meanwhile, integrating OET with DMF facilitates precise manipulation of particles in a single or multiple droplets. By programming the operation of droplets, this approach shows advantages in flexibility, scalability, and automation[39]. However, it requires complex system designs, advanced chip fabrication, and a fully integrated control system. Furthermore, OET-OEW microfluidics show unique advantages in particle and droplet manipulation [40,46-49]. This approach allows a simultaneous control of particle manipulation and droplets behavior, including droplet merging, droplet splitting, and encapsulation of single cells into droplets. Despite these advancements, further improvements are needed in system stability and the integration of multiple detection/characterization modules to enable practical applications. Overall, the precise manipulation capabilities of OET at low optical power and easer of parallelization align perfectly with the increasing automation demands in microfluidics.

With further integration with artificial intelligence (AI) algorithms for image recognition and path planning, OET holds great promise in micromanipulation in microfluidic chips, facilitating parallel or serial target operations[50].

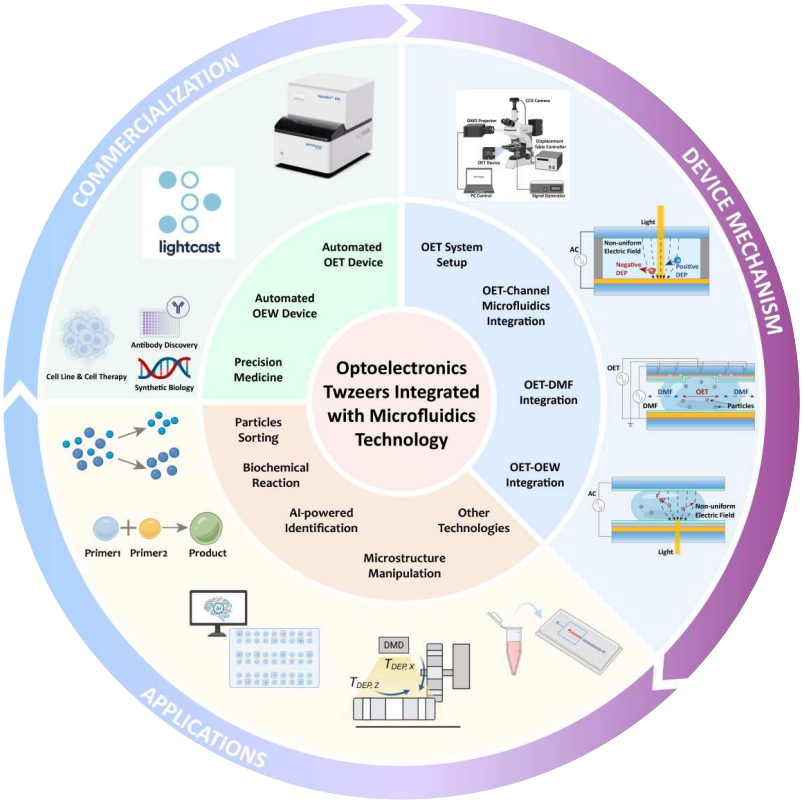

Fig. 1 Schematic of the integration of OET with microfluidics, including device mechanism, application, and commercialization.

In this review, we provide a comprehensive overview of the fundamentals, applications, and commercialization of OET with microfluidics, as shown in Fig. 1. First, we present an overview of main integration approaches, focusing on the strategies and features of combining OET with microfluidic techniques, including channel microfluidics, DMF, and OEW microfluidics. Next, we delve into the working mechanisms of OET within channel (continuous flow) microfluidic platforms, highlighting its mechanisms and summarizing typical

applications, such as the sorting of abiotic particles[51-53], microstructure assembly[54-58], and biomedical analysis[59,60]. We then examine the integration of OET with DMF and OEW, emphasizing its potential in microdroplet manipulation[61-66], single-cell manipulation[67-72], and high-throughput cell/particle screening[73-76]. Additionally, we provide a thorough overview of the current development of OET-microfluidic integrated systems in industrial applications, particularly in drug development and discovery. Finally, we explore the commercialization of optoelectronic microfluidic technologies and discuss future directions and potential breakthroughs based on current research trends.

II. OET Fundamentals

The development of OET emerged as an advancement and inspiration of optical tweezers (OT) [1,2,17]. In 2005, the concept of OET was formally established, aiming to achieve precise manipulation of microparticles through the joint use of optical and electric fields[3]. OET manipulates objects at the nano- and micro- scales by projecting light patterns onto a photoconductive semiconductor substrate to locally generate electrokinetic forces[77-80]. This section will review the experimental setup and the working mechanism of the OET technique.

2.1. Components of OETs and the Experimental Setup

In the past decades, various OET devices have been developed to enhance the precision and flexibility of trapping and manipulation. A standard OET system consists of several key components[43], including a digital micromirror device (DMD) projector with integrated or external light source, a microscope, a function generator for producing AC voltages, an AC amplifier, a positioning stage (preferably motorized), and a computer (Fig. 2a). The DMD projector generates a programmable light pattern being projected through an objective lens onto the photoconductive layer of the OET device. This can be done through the microscope or using custom optical arrangements. These light patterns induce the virtual electrodes that will create the non-uniform AC electric field which generates gradient force for trapping and manipulation. A microscope equipped with a camera and filters is used for imaging in real time to observe of

the manipulated objects. This visual feedback from the microscope can be used to adjust the light's wavelength and intensity in real time, ensuring sufficient optical power for effective manipulation. The microscope imaging can be done with the same objective lens as the projection by using a beam-splitter/dichroic to split the illumination and imaging paths. A dual objective setup can also be used where the projection and imaging are done using separate objective lenses[81]. The function generator produces an AC signal, which is amplified by the amplifier to drive the OET device. This amplified voltage is applied across a reference electrode, usually an ITO coated glass coverslip located at the top of the suspension medium, and a planar transparent electrode located below the photoconductor (Fig. 2b). Note that this is the arrangement of the most commonly used vertical field OET devices. For lateral field OETs and other custom OET setups, the arrangement of the reference and the photoconductor electrodes differ. However, all OETs use the same basic principle of modifying the background AC electric field between two sets of electrodes using light patterns projected on a photoconductor that lies between those electrodes. The OET device usually sits on a motorized positioning stage that precisely controls the position device, allowing for either movement of the device or relative translation between the light pattern and the device to manipulate the object[82-84]. The precise control it provides further facilitates detailed studies of the movement speed and manipulability of objects.

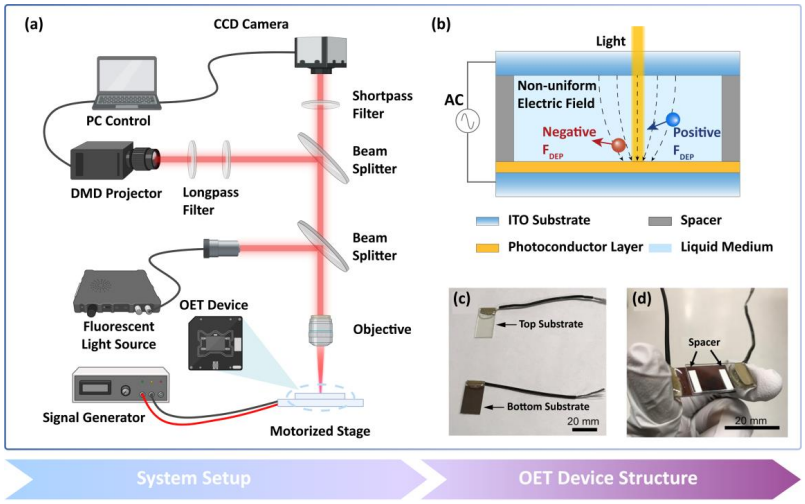

Fig. 2. Principles of the OET. (a) Experimental setup. (b) Schematic diagram of the OET device. (c) The top and bottom substrates of the OET device. (d) The assembled OET device. (c-d) Reproduced from ref. 108 with permission from John Wiley and Sons, copyright 2019.

The OET system is flexible in variating translation speeds for different manipulation forces or moving objects along complex trajectories using animated light patterns[85-89]. Additionally, the OET system can manipulate thousands of cells or particles simultaneously over a large field of view, making it suitable for high-throughput sorting[90]. This is made possible by the DMD, which can project multiple independent light patterns and control them independently. Since OETs work with low power, dividing the total power of a light source into multiple sub-patterns by the DMD still provide sufficient optical power for OET operation. Beyond micromanipulation, the system can be integrated with various techniques such as Raman spectroscopy[91], reflection spectroscopy[92], UV photo-curing system[44], and microfluidics[93], enabling a wide range of applications. In these systems, all manipulation and detection analyses are conducted in suspension media with different electrical properties. The medium is usually selected to make it suitable for the target specimen. The shape of the light

field is programmed to achieve precise manipulation of the target, thanks to a stable fluid environment.

The integration of OET with microfluidics fundamentally enhances manipulation capabilities by introducing a precisely controllable fluid environment. Firstly, microfluidic channels provide a physically confined and stable liquid medium, which significantly improves the precision and repeatability of optical capture, sorting, and positioning. Secondly, by introducing a continuous laminar fluid flow, the system can leverage hydrodynamic forces to transport specimens at high speeds, dramatically increasing the processing throughput beyond the limits of optical transport alone. To achieve this goal, a fluid control architecture is required, including external electrodes, injection pumps and pressure controllers, as well as fully integrated on-chip microvalves and pumps. Therefore, the combination of a dynamic optical landscape and a managed fluidic environment is critical for developing high-efficiency, high-throughput micromanipulation platforms.

As shown in Fig. 2b, the schematic diagram of the OET device illustrates its operational mechanism. The device is consisted of a top and a bottom glass substrate, each coated with indium-tin-oxide (ITO). The space between the substrates forms a reservoir for the manipulated objects and the liquid medium[94]. The bottom substrate is further coated with a photoconductive layer, such as hydrogenated amorphous silicon (a-Si:H), Titanyl phthalocyanine (TiOPc) [95-97], bulk heterojunction (BHJ) polymers[98,99], Lithium niobate crystal（$LiNbO_3$）[100–103]，or silicon-based phototransistors[104,105].

The operational principle of OET is founded on light-induced AC electrokinetics, where projected optical patterns create dynamic, virtual electrodes to exert forces. The core mechanism begins when photons with energy exceeding the photoconductor's bandgap are absorbed, generating free electron-hole pairs. This influx of photogenerated carriers dramatically increases the local electrical conductivity in the illuminated regions. In an OET device, an AC electric field is applied across a sandwich structure comprising the photoconductor and a liquid medium containing the microparticles. In the dark, the photoconductor has high impedance, causing most of the voltage to drop across it and leaving

a weak, uniform field in the liquid. However, upon illumination, the localized increase in conductivity effectively shunts the AC voltage to the liquid layer, creating a strong, non-uniform electric field that spatially mirrors the light pattern. This non-uniform field induces a dipole moment in the suspended particles, and the interaction between this dipole and the field gradient generates a net dielectrophoretic (DEP) force that enables manipulation. The efficiency of this process is intrinsically linked to the material's absorption spectrum. For instance, a-Si:H exhibits a high absorption coefficient at shorter wavelengths in the violet-blue region, making such light highly effective for generating strong DEP forces[106,107]. It should be noted that due to the broad absorption spectrum of a-Si:H in the visible wavelengths, broadband white light sources can also be used.

A user-defined light pattern is projected onto the surface of the photoconductive layer through the DMD, while electrical leads are connected to the ITO electrodes on both substrates (Fig. 2c). The device is then assembled by enclosing the components within a chamber (Fig. 2d)[43]. Liquid medium containing objects is introduced into the chamber through injection holes[108]. An external AC electrical signal is applied to the top and bottom surfaces of the OET device through connected wires[106]. The amplitude, frequency, and waveform of the AC signal can be adjusted for a given target specimen. Typically, AC bias is applied at frequencies ranging from a few kHz to several hundred kHz[109]. The frequency is selected for the specific application[110]. The waveform shape is usually selected as sinusoidal, however, an OET device produces the maximum manipulation force when powered by a square-wave AC bias for a given voltage and frequency.

To generate the required manipulation force, the medium's impedance must fall between the impedance of the illuminated photoconductive state and that of the dark state. Thus, the conductivity of the liquid medium is in a permissible range defined by the impedance matching factor[109,111]. The optimal dielectric conductivity of the liquid is generally close to the square root of the product of the conductivities of the light and dark states of the photoconductor material. The conductivity of the photoconductor and the frequency of the applied voltage also

influence the lower limit of the dielectric conductivity. In low-frequency conditions, a liquid with lower conductivity may be used.

2.2. Physical Mechanism of OET

The DEP is an electrodynamic phenomenon in which a polarizable object moves in a non-uniform electric field. This DEP force is typically the dominant force in OET-based manipulation. The strength of the DEP force depends on the electrical properties of both the liquid medium and the object, as well as the frequency and amplitude of the applied alternating electric field[112,113]. In OET, the DEP force is generated through the projection of a light pattern, a process referred to as optically induced dielectrophoresis (ODEP; in this article, DEP that is induced by the OET phenomenon is consistently written as ODEP).

To calculate the ODEP force, two methods are commonly used according to the shape of the object. In OET, spherical particles are most frequently manipulated, and the classical dipole approximation is typically applied to calculate the ODEP force. The time-averaged ODEP force acting on a spherical particle in a liquid medium is defined as[107,114-117]:

$$F_{ODEP} = 2\pi r^3 \varepsilon_m \,\mathrm{Re}[K(\omega)]\,\nabla|\boldsymbol{E}|^2 \quad (1)$$

where r is the radius of the spherical particle, εm is the dielectric constant of the liquid medium, ω is the angular frequency of the applied AC voltage, $|\boldsymbol{E}|$ is the root-mean-square (RMS) value of the inhomogeneous AC electric field, and Re[$K(\omega)$] is the real part of the Clausius-Mossotti (CM) factor. In the context of OET, the polarization of a spherical particle in relation to the surrounding liquid medium are represented by the CM factor, which is defined as follows[114,115]:

$$K(\omega) = \frac{\varepsilon_p' - \varepsilon_m'}{\varepsilon_p' + 2\varepsilon_m'} \quad (2)$$

In the context of electromagnetics, the complex permittivity of a spherical particle is denoted as ε_p'. The complex permittivity of the liquid medium is indicated by ε_m'. The expressions for these complex dielectric constants are provided below for reference:

$$\varepsilon_p' = \varepsilon_p - j\frac{\sigma_p}{\omega} \quad (3)$$

$$\varepsilon_m' = \varepsilon_m - j\frac{\sigma_m}{\omega} \quad (4)$$

In this equation, j represents the imaginary vector, ε_p and ε_m denote the dielectric constants of the spherical particles and the liquid medium, respectively. The σ_p and σ_m represent the conductivities of the spherical particles and the liquid medium, respectively.

The direction of the ODEP force applied to a spherical particle, as described in Eq. (2), is determined by the polarity of the real part of Re[$K(\omega)$]. When Re[$K(\omega)$] > 0, a positive ODEP force is generated, driving the particle to move from areas with low electric field strength (dark regions) to areas with high electric field strength (light regions). So, particles are trapped in the illuminated region. This phenomenon has been utilized to enrich extracellular vesicles（EVs）within continuous microfluidic channels[118]. Conversely, when Re[$K(\omega)$] < 0, a negative ODEP force is generated, driving the particles away from regions of strong electric fields. This phenomenon is commonly employed in microfluidics for sample separation, such as selectively capturing cells from a mixture and transporting them into a small chamber for isolation[68,119-122]. Trapping can still be achieved using negative ODEP with a ring-shaped light pattern. The repulsive force from the illuminated region around the circumference traps a particle in the dark region at the center. At the critical point where Re[$K(\omega)$] = 0, the ODEP force is zero, indicating the equilibrium. The corresponding driving frequency is known as the crossover frequency, which serves as an important indicator for distinguishing the dielectric properties of different cells[123].

While CM factor provides an intuitive framework for understanding the influence of experimental parameters on the DEP force, its applicability is limited by simplifying assumptions and a lack of quantitative capability[124]. For example, it assumes the particle size is significantly smaller than the special scale of the field's inhomogeneity (i.e., point particle approximation), and that the DEP force acts uniformly across the particle. However, experimental results frequently disagree with these assumptions. A more precise model for the DEP force on an object can be formulated using the Lorentz law of force in conjunction with the Maxwell stress tensor, as follows[122,125,126]:

$$\overleftrightarrow{T}_{ij} = \varepsilon_0 \boldsymbol{E_i E_j} + \frac{1}{\mu_0}\boldsymbol{B_i B_j} - \frac{1}{2}\left(\varepsilon_0 |\boldsymbol{E}|^2 + \frac{1}{\mu_0}|\boldsymbol{B}|^2\right)\delta_{ij} \quad (5)$$

The $\overleftrightarrow{T}_{ij}$ element of the second-order Maxwell stress tensor, ε_0 and μ_0 are the vacuum capacitance and magnetic permeability, respectively. The electric and magnetic fields are represented by $\boldsymbol{E}$ and $\boldsymbol{B}$, respectively. The Kronecker's delta is defined as δ_{ij}. Integrating the Maxwell stress tensor over the surface area eclosing the dielectric object yields the total DEP force acting on the object within the electromagnetic field [84,125,126].

$$F_{DEP} = \int_s \overleftrightarrow{T} \cdot \hat{n} dS \quad (6)$$

It should be noted that this equation is derived from the effective dipole approximation, a model that provides accurate results when the particle can be treated as an ideal point dipole. While this simplification is effective for isotropic spheres where higher-order multipole effects are negligible, its validity diminishes for particles with complex geometries, such as ellipsoidal erythrocytes. For a universally rigorous analysis applicable to particles of arbitrary shape and material composition, the Maxwell Stress Tensor (MST) method provides a more fundamental and accurate approach. By integrating the electromagnetic stress over a surface enclosing the particle, the MST directly calculates the net force, inherently accounting for complex geometries and non-linear material properties without the limiting assumptions of the dipole model. In such cases, the momentum change of the particle can be characterized as:

$$\Delta \boldsymbol{p} = \left[\int_V (\boldsymbol{P} \cdot \nabla)\boldsymbol{E} + \mu_0 (\boldsymbol{J} \times \boldsymbol{B})\right] dV \quad (7)$$

It is critical to consider the impact of particle geometry on the polarization strength (P) and electromagnetic field distribution. These calculations are typically performed using finite element simulation software. In experimental studies, the precise manipulation of non-spherical cells is achieved by light-induced dynamic electric field modulation.

While the primary manipulation force in OET arises from the ODEP interaction between an object and a non-uniform electric field, a complete understanding of the system requires acknowledging secondary phenomena. The incident light can also induce localized thermal gradients, which in turn drive fluid motion and particle transport through the AC electrothermal (ACET) [107,127,128]. A notable advantage of employing a-Si:H as the photoconductive layer in

OET is its inherent ability to minimize undesired photothermal effects. The material's wide bandgap (~1.6–1.8 eV) ensures efficient photogeneration of charge carriers under visible illumination while limiting the conversion of optical energy into excess heat. Since most of the light is absorbed by a-Si:H, the sample is exposed to very small amount of optical energy which reduced possibility of photothermal damage for even the most sensitive biosamples. In practice, the sub-micrometer film thickness provides strong conductivity modulation yet is thin enough to suppress thermal accumulation. Furthermore, OET operates at low optical intensities (0.1–1 W/cm²), several orders of magnitude lower than conventional optical tweezers, which drastically reduces the thermal load on the sample. Any residual heat dissipates efficiently through the substrate and liquid medium, keeping local temperature increases negligible (< 1–2 °C). These collective attributes enable a-Si:H based OET systems to provide robust field modulation while preserving the cell viability and biochemical integrity essential for single-cell manipulation and proteomics. Concurrently, the interaction of the electric field with the induced double layer at the electrode surfaces generates fluid flow via AC electroosmosis (ACEO) [107,128-130], while the field's action on charged particles produces electrophoretic (EP) motion[115,131]. Although these secondary electrokinetic effects, along with non-specific adhesion, can influence manipulation, their contributions are often secondary to the dominant ODEP force in typical OET applications. To optimize the performance of OET systems, it is essential to fully understand and exploit these mechanisms. In microfluidic applications, the primary manipulation is achieved through dielectrophoretic effects, so this paper will focus on ODEP force generated by OET without delving deeply into the influence of other effects on manipulation.

While the low optical power density required for OET minimizes direct photothermal damage—a distinct advantage over traditional optical tweezers—thermal management remains a critical physical constraint due to volumetric Joule heating. This effect becomes particularly pronounced when operating in high-conductivity physiological buffers (σ> 1 S/m) or under high-frequency AC fields. The volumetric heat generation rate is governed by $Q = \sigma|E|^2$, where σ is the fluid conductivity and E is the local electric field. During micromanipulation,

this continuous energy dissipation leads to localized heat accumulation. Beyond the direct risk of inducing thermal stress or heat-shock responses in sensitive biological targets, the resulting spatial temperature gradients (∇T) induce local variations in the fluid's permittivity ($\partial\varepsilon/\partial T$) and conductivity ($\partial\sigma/\partial T$). These gradients trigger electrothermal flows (ETF), creating viscous drag forces that actively compete with the DEP trapping potential, potentially destabilizing the manipulation regime. To mitigate these coupled electro-thermal-hydrodynamic effects without compromising the manipulation force, temporal modulation strategies are employed. By utilizing pulsed light patterns rather than continuous illumination, the system actively manages the energy duty cycle, significantly reducing the time-averaged thermal load while maintaining the threshold electric field required for stable target confinement.

Ultimately, the necessity of actively managing this thermal load highlights the unique multiphysics nature of the platform. OET must mitigate the Joule heating originating from the global alternating current electric field, particularly in highly conductive physiological buffers. However, its localized optical energy footprint remains fundamentally negligible. To fully appreciate this advantage, and to contextualize OET within complex biological applications, it must be quantitatively benchmarked against its two foundational predecessors: conventional OT and traditional metal-electrode-based DEP. The core distinction among these platforms lies in their energy-to-force transduction mechanisms, spatial resolution, and resulting thermal footprints.

OT relies on the direct linear momentum transfer from photons to dielectric objects[132-134]. This extreme spatial precision makes OT the gold standard for high-bandwidth force spectroscopy and intracellular surgery—such as the targeted extraction of organelles using thermoplasmonic-enhanced optical trapping[135]. As highlighted by recent state-of-the-art advancements, OT is uniquely capable of executing sub-cellular targeted drug delivery[136-139], probing intracellular mechanics at the nanometer scale, and manipulating active living micromotors[140,141]. However, this radiation pressure regime requires extreme optical intensities (10^5 – 10^7 W/cm²) to overcome Brownian fluctuations. In aqueous biological media, this high photon flux density frequently induces localized photothermal temperature rises (ΔT) of several

to tens of degrees Celsius, posing a severe risk of nonlinear photodamage to sensitive targets during manipulation.

Table 1. Comparison of OT, Conventional DEP, and OET

Feature	Optical Tweezers (OT)	Conventional DEP	Optoelectronic Tweezers (OET)	Ref.
Physical Mechanism	Direct photon momentum transfer	Non-uniform AC electric field	Optically-induced dielectrophoresis (ODEP)	3,18,114
Required Light Intensity	High (10^5 – 10^7 W/cm²)	N/A (Electrically driven)	Low (10^0 – 10^2 W/cm²)	3,114,132
Typical Force Magnitude	pico-Newton (pN)	nano-Newton (nN)	nano-Newton (nN)	132,142,256
System Flexibility	Dynamic (Steerable laser)	Static (Fixed metal electrodes)	Highly Dynamic (Programmable virtual electrodes)	146,256
Manipulation Scale	Single or few targets	Bulk populations	Massively parallel (Up to 10^4 targets)	2,3,145
Target Size Range	10 nm to 20 μm	> 1 μm	1 μm to 500 μm	115,133,144
Biocompatibility	Risk of photothermal damage	High (Subject to Joule heating)	High (Minimal optical/thermal footprint)	134,143,256

Conversely, conventional DEP generates robust nano-Newton (nN) scale forces using localized AC electric fields, entirely avoiding optical photothermal damage[142,143]. This makes it highly effective for massively parallel bulk cell sorting[144,145]. Yet, conventional DEP is physically constrained by prefabricated metal electrodes, which rigidly fix the manipulation trajectories and severely limit dynamic, single-cell spatial resolution[115,146]. OET uniquely bridges this technological gap by leveraging the photoconductive gain of semiconductor substrates. By using incident light merely as a spatial switch to modulate the interfacial impedance, OET redistributes the external electrodynamic potential into highly localized DEP profiles. It achieves the massively parallel manipulation and nN-scale forces of conventional DEP, but with the profound advantage of dynamically programmable 'virtual electrodes'. Most

critically for biological applications, this actuation requires optical power densities five orders of magnitude lower than OT (~ 10^0 – 10^2 W/cm²), restricting the maximum photothermal temperature rise to well below 1 ℃.

Interestingly, this introduces a multiphysics duality inherent to OET platforms. While an absolute bulk ΔT < 1 ℃ is thermodynamically benign and ensures exceptional cellular viability, the spatial distribution of this minimal heat generation creates highly localized thermal gradients (∇T) at the edges of the optical illumination patterns. Because the scaling forces of ACET flow depend fundamentally on the temperature derivatives of the fluid's permittivity ($\partial\varepsilon/\partial T \approx$ -0.4% /℃) and conductivity ($\partial\sigma/\partial T \approx$ +2% /℃), even these fractional-degree spatial gradients—when coupled with a strong local AC electric field are sufficient to induce localized ACET micro-vortices. Thus, the localized photothermal gradient in OET serves as an electro-hydrodynamic boundary condition that must be actively managed for stable trapping, but it avoids the biological thermal hazards associated with traditional optical manipulation with laser[115].

Beyond simple trapping, this biologically benign thermal footprint and high-throughput nature allow OET-based systems to excel in massively parallel bioprocessing. By coupling light-induced fields with biological carriers, OET has evolved into a platform for navigating living micromotors and microrobots for targeted bio-threat removal and precision neural modulation. Thus, this unique synergy combines the high-throughput nature of DEP, the dynamic reconfigurability of OT, and a biologically benign thermal footprint, establishing OET as a powerful platform that bridges the gap between single-target sub-cellular manipulation and large-scale, non-invasive biochemical analysis.

2.4 The Conductivity Challenge in Physiological Media

A fundamental operational boundary of OET platforms is the stringent impedance matching requirement between the solid-state photoconductor and the fluidic medium[111]. The system inherently functions as an optically modulated voltage divider; to establish a trapping potential, the fluid's impedance must lie strictly between the dark and illuminated impedances

of the semiconductor layer. However, standard physiological buffers and cell culture media (e.g., phosphate-buffered saline) typically exhibit high electrical conductivities ($\sigma > 1$ S/m), resulting in a profoundly low bulk liquid impedance. In this regime, the 'conductivity challenge' manifests through two coupled physical degradation pathways. First, the voltage drop across the liquid layer becomes negligible, even under peak optical illumination. Second, the high ionic strength severely compresses the Debye length, leading to the formation of a dense electrical double layer (EDL) at the solid-liquid interface. This EDL induces a strong field screening effect that confines the potential drop to the nanometer-scale interface, fundamentally suppressing the effective ODEP force in the bulk fluid.

To circumvent this physical bottleneck and enable deterministic biological manipulation (such as single-cell sorting or dynamic cell-killing assays), two primary strategies are currently employed. The most immediate thermodynamic approach involves the formulation of low-conductivity, iso-osmotic buffers. By substituting ionic salts with non-ionic osmolytes such as sucrose or mannitol, the bulk conductivity is reduced to an operational window ($\sigma \sim 10^{-2}$ S/m) while maintaining osmotic pressure. While highly effective for force generation, prolonged exposure to these atypical, ion-depleted environments may perturb sensitive cellular metabolism.

Alternatively, to operate directly in high-conductivity media without sample dilution, architectural innovations such as phototransistor-based OET platforms have been developed[71,105]. These complex multi-layer semiconductor structures provide intrinsic signal amplification, enhancing the localized photoconductive gain sufficiently to penetrate the EDL screening. By amplifying the injected current, these advanced architectures sustain effective ODEP force even in raw physiological fluids, representing a critical hardware evolution for the future of clinical OET applications.

III. OET-Channel Microfluidics Integration

In this section, we provide an overview of the integration of OET technology with channel microfluidics. We will detail the chip design, and discuss their working mechanisms and applications, particularly in the biomedical field.

3.1. Integration and Working Mechanism

The integration of OET with channel-based microfluidics offers an efficient approach for the manipulation and sorting of nanoscale particles[147,148]. With the combined effects of the OET and the microfluidic structures, researchers can achieve precise capture[149,150], enrichment[151-153], sorting[154-156], and directional transport of biological (e.g., cells, bacteria, exosomes) or functional particles in a nicely controlled fluidic environments[157-161]. Furthermore, this paradigm extends beyond simple particle handling to enable dynamic, reconfigurable control over the microfluidic functions themselves. By precisely assembling the manipulated particles or cells at desired locations, it is possible to form functional microstructures on-demand, such as temporary valves, programmable filters, or dynamic biological arrays, effectively using the target samples as active components of the device.[93,162,163].

In channel microfluidic systems, the manipulated objects typically range from tens of nanometers to hundreds of micrometers in size. Fig. 3a-b illustrate a microfluidic system for particle collection and enrichment, where OET generates an array of light traps through high-precision optical field modulation. The interaction between photogenerated virtual electrode induced non-uniform electric field and dielectric particles produces attractive or repulsive forces, with the direction determined by the dielectric constant of the particle relative to the surrounding medium. Classical theories, as discussed in Section 2.2, can be used to explain the behavior of polystyrene microbeads under OET manipulation[82,163,164]. A key strength of this technology is the ability to exert precise real-time control over the resulting ODEP forces. This is accomplished by dynamically modulating the light patterns projected by a DMD, which enables instantaneous adjustment of the position, size, shape, and intensity of the optical traps. To enhance the enrichment efficiency, the OET traps is periodically switched on and off in sync

with fluid flow in the microchannels, which is especially useful for pretreatment of rare samples. Alternatively, the size of light traps can be reduced to compress the particles into a compact area for enrichment. The captured particles are then assembled and analyzed. In the microstructure array (Fig. 3b), periodically arranged microcolumns or microcavity structures are incorporated into the main channel. Each unit is designed to match the size of the target particles. In this integration approach, a composite "physical-OET" trap is formed. As particles flow through the device, they are initially intercepted by dynamic OET traps, which subsequently deliver them into physical traps. These traps consist of static, microfabricated structures such as wells or notches, which are designed for stable confinement. This significantly improves the particle capture efficiency and stability, making it particularly suited for biological cell fusion and high-throughput screening[151,153].

Another application of OET-channel microfluidic integration is particle classification based on differences in physical properties. Fig. 3c illustrates a microfluid chip with sidewalls of the main channel connected to multiple lateral branching microchannels. This design incorporates a dynamically rotating light pattern for selective capture, based on the variation in ODEP forces for different particles. Unselected particles are directed to the collection area with the fluid flow direction. The system utilized both the ODEP forces and fluidic forces to pre-select target particles, directing them to distinct side channels for particle size grading. This technique has been successfully applied in immunocyte sorting[165-168], where cells with different surface markers are sorted into separate channels for subsequent analysis.

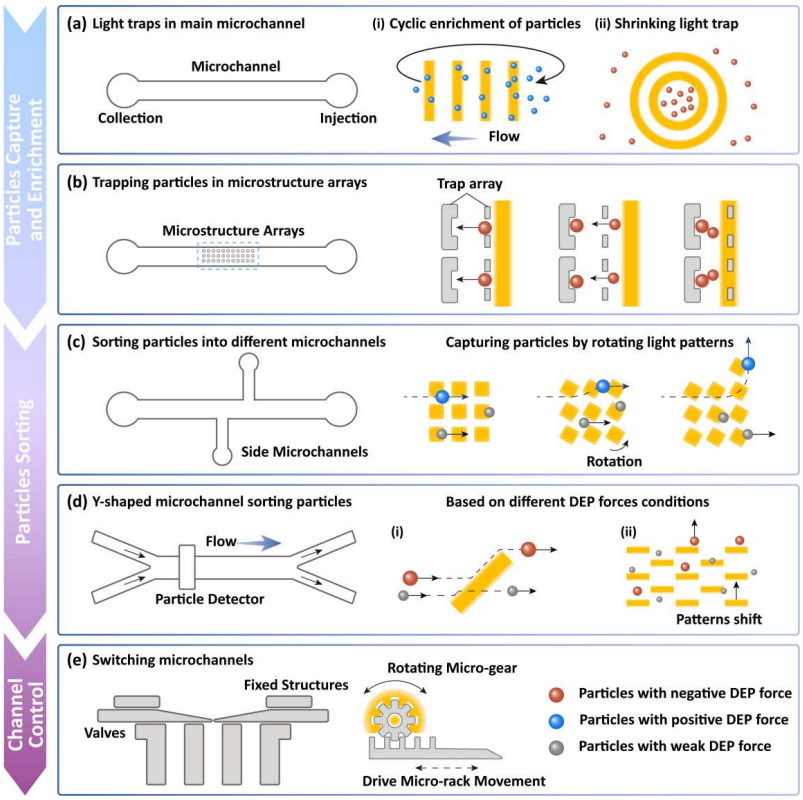

Fig. 3. OET integrated with channel microfluidics. (a) Circulation of liquid within the microchannel for particle screening or narrowing the spot for particle enrichment. (b) Trap array in the microchannel transports particles into physical traps through ODEP forces. (c) Particle sorting through spot rotation and translation based on the different ODEP force applied to different particles. (d) In a Y-shaped microfluidic channel, particles are sorted to different outputs using a combination of fluidic and ODEP forces. (e) Microchannel switching controlled by OET-directed micromechanical actuators.

To further increase the throughput of particle sorting, researchers have employed a microchannel with a Y-shaped bifurcation structure, combined with DEP forces to sort particles (Fig. 3d). In this system, the light pattern is defined as an angled ramp or a cyclically ascending ladder. Particles subjected to negative ODEP forces are repelled to one side of the microchannel,

while those with positive ODEP forces follow the fluid flow into the other side. Integrated particle detectors in the main channel analyze the sorting results in real-time and implement closed-loop control by dynamically adjusting the electric field frequency or OET parameters, enabling high-efficiency, accurate sorting. While electrode based conventional DEP systems can also be used for such applications, OET provides a layer of flexibility as the light-induced virtual electrodes can be dynamically adjusted to fine tune the device operation.

Direct manipulation of microfluidic components by OET offers a promising tool for developing more complex and highly integrated micromechanical systems (Fig. 3e). The combination of OET and microfluidics not only enables high-precision manipulation but also facilitates multi-dimensional sorting using multiple parameters, such as particle size, dielectric constant, or surface antigens, through parallel processing with minimal sample consumption using on-chip detection/characterization schemes. This integration has been applied in precision medicine (e.g., CTC sorting, stem cell sorting, pathogen detection)[93,155,165-168], synthetic biology (e.g., microparticle synthesis, artificial cell assembly)[45,153,169,170], and environmental monitoring (e.g., rapid microbial detection, contaminant separation)[154,171]. As chip integration and automation advance, the combination of OET with microfluidics is poised to become important tools for life science research and clinical diagnostics[92,172-174].

Following the development of OET, researchers recognized the importance of integrating OET with microfluidics as an advancement of standard lab-on-a-chip systems with electrode-based DEP. The key to this integration lies in the design of geometries within the OET manipulation region, enabling precise fluid control[175,176]. This integration facilitates continuous sample delivery and extraction within microstructures, supporting high-throughput sorting, separation, and processing of targets. A critical aspect of combining a channeled microfluidic device with OET is the creation of a microchannel feature layer, connecting the OET's top and bottom substrates to form a closed channel. Common materials for the feature layer include double-sided tape, UV-curable polymers, and polydimethylsiloxane (PDMS)[177,178].

Double-sided adhesive tape is vital in OET device fabrication, serving as the bond between the transparent conductive ITO glass layers and forming the microfluidic channel framework

(Fig. 4a)[179]. Fig. 4b displays an OET device with microfluidic channels. The tape layer, 30 μm thick, is shaped using laser cutting technology. The tape is securely bonded to the ITO glass through a rolling process, ensuring structural integrity and stability. This design simplifies fabrication and significantly reduces processing time. However, limitations exist, as laser cutting may compromise the precision of the microchannels due to burned or melted edges. To resolve this, hollow microchannels were manually stamped onto the tape using a custom metal die, and a high-resolution cutter was then employed to improve precision, yielding cleaner cuts and finer details. Overall, these methods for creating microfluidic channels on double-sided tape are simple, cost-effective, and mitigate contamination risks associated with photolithography or etching processes, making this approach widely adopted in OET-microfluidic integrations.

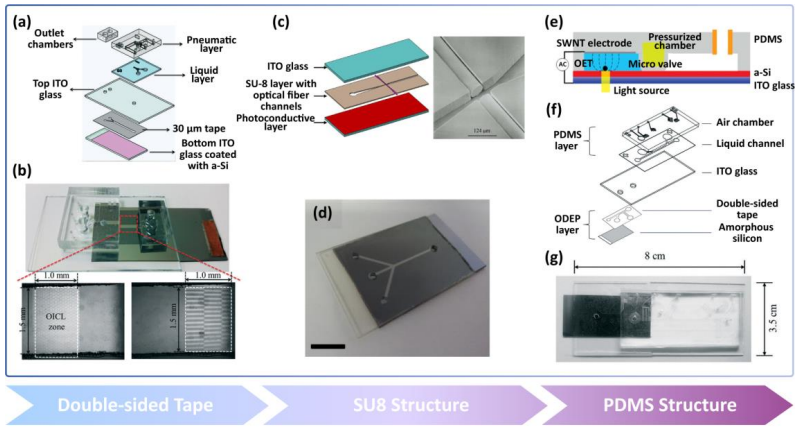

Fig. 4. Different strategies to integrate OET device with channel microfluidics. (a) Schematic illustrating the structure of the OET microfluidic device, which utilizes double-sided tape and microchannels. The microchannel structure is fabricated by laser cutting the double-sided tape. (b) Image of the OET microfluidic device, featuring a flow control module, an OICL module, and an ODEP module. (a and b) Reproduced from ref. 179 with permission from Royal Society of Chemistry, copyright 2016. (c) Schematic of the OET microfluidic chip design, which includes SU8 microchannels and a pair of fiber optic detection devices, accompanied by SEM

552 images. Reproduced from ref. 180 with permission from Elsevier, copyright 2008. (d) Image
553 of the OET microfluidic device, featuring Y-shaped microchannels made from SU8.
554 Reproduced from ref. 45 with permission from IOP Publishing, copyright 2020. (e) Schematic
555 of the OET microfluidic device design, incorporating a PDMS top substrate and PDMS
556 microchannels. Reproduced from ref. 177 with permission from Royal Society of Chemistry,
557 copyright 2013. (f) Schematic of the OET microfluidic device structure, which combines
558 double-sided tape and PDMS. (g) The OET device consists of a PDMS fluidic channel
559 integrated with both the OET module and a double-sided tape microfluidic module. (f and g)
560 Reproduced from ref. 162 with permission from Royal Society of Chemistry, copyright 2016.
561
562 Microfabrication with UV-curable polymeric materials is a widely adopted method for
563 fabricating microfluidic channels, wherein SU-8 photoresist plays a pivotal role in creating
564 high-resolution structures. As depicted in Fig. 4c, a representative OET device incorporates a
565 microchannel composed of an SU-8 layer, which is patterned through photolithography to form
566 a Y-shaped structure[180]. This SU-8 layer is usually directly patterned onto ITO-coated glass
567 substrates, capable of precisely forming microstructures of tens of micrometers in size to adapt
568 to various flow rates and particle sorting applications. Furthermore, this microchannel can be
569 integrated with optical detection fibers to enable hydrodynamic cell focusing and counting. SU-
570 8 is advantageous due to its capacity for high-resolution structuring, allowing it to accurately
571 replicate complex channel designs while providing robust mechanical strength. Moreover,
572 additional components for detection and sample modification can be incorporated into the
573 channel, further enhancing the system's functionality.
574 An alternative method developed by Witte et al[45], involves a multi-layer spin-coating of
575 photoresist on the OET substrate (Fig. 4d). Although effective, this method presents challenges
576 in fabricating high-resolution microchannels, and the complete fabrication process can be time-
577 consuming, often requiring several days. Beyond SU-8, other UV-curable polymers, such as
578 poly (ethylene glycol) diacrylate (PEGDA), are also employed in microfluidic fabrication. In

this approach, a prepolymer solution is sandwiched between two substrates and exposed to UV light, enabling the rapid formation of microchannels, often within seconds.

The PDMS is another key material for fabricating microfluidic channels due to its excellent biocompatibility and optical transparency. PDMS microfluidic structures are usually fabricated using "soft-lithography" from a physical mask usually made of SU8. This process is simple and inexpensive compared to photolithography, making PDMS one of the most popular materials for microfluidic applications. To use PDMS for OET, ways of incorporating electrical contacts in the systems must be developed. In some device architectures, OET electrodes have been fabricated by embedding single-walled carbon nanotubes (SWNTs) into a multi-layer PDMS structure. Fig. 4e illustrates an OET device integrated with pneumatic control channels within a PDMS microfluidic architecture[177]. In this design, PDMS microchannels are fabricated using soft lithography. The top OET electrode is subsequently formed by spin-coating an uncured PDMS precursor onto a transfer die and infiltrating it into an SWNT network matrix. This creates a conducting electrical contact while maintaining optical transparency for imaging. The complete device is assembled by bonding the bottom photoconductive substrate to the multilayer PDMS structure using an oxygen plasma treatment, which ensures a hermetic seal. Such multi-layer PDMS architectures can integrate pneumatic valves, enabling complex, multi-step sample preparation for single-cell analysis.

To streamline the integration of sophisticated PDMS-based microfluidics, which involves multi-step soft lithography, a modular fabrication approach offers a highly effective solution (Fig. 4f)[162] . This strategy involves fabricating a PDMS-based fluidic control module separately, which is then directly bonded onto the OET processing module. Such a stacked integration synergistically combines the robust fluidic control of PDMS with the high-precision micromanipulation capabilities of OET, establishing a versatile platform for continuous cell sorting and processing as depicted in Fig. 4g[162].

On the manufacturing front, scalability represents the primary bottleneck hindering widespread commercialization. The path forward requires a fundamental shift away from costly, low-throughput cleanroom processes toward scalable manufacturing paradigms adopted from

607 fields like flexible electronics. This approach involves leveraging solution-processed
608 optoelectronic materials, such as organic semiconductor or quantum dot inks, in conjunction
609 with high-throughput printed electronics techniques like roll-to-roll (R2R) and inkjet printing.
610 These methods are ideally suited for fabricating devices on low-cost, flexible polymer
611 substrates, a transition that promises to reduce per-chip costs by several orders of magnitude.
612 Ultimately, this paradigm shift in manufacturing is the key to enabling the mass production of
613 disposable, single-use chips, an essential prerequisite for their adoption in clinical diagnostics
614 and point-of-care testing (POCT).
615
616 **3.2. OET-Channel Microfluidics-based Micro/Nanoscale Manipulation**
617 OET has been widely used to manipulate and assemble a diverse range of nano- and micro-
618 scale materials, including conductive nanoparticles[181,182], cell secretions[154],
619 semiconductor/metal nanowires[108,183,184], plastic microspheres[83,84,185,186], metal particles[187-189],
620 and microrobotics[190-193]. OET enables the simultaneous parallel manipulation of multiple
621 targets, as well as the movement of large objects, ranging from tens of nanometers to several
622 hundred micrometers in size.
623 The OET-pneumatic microchannel integrated device enables label-free, non-contact
624 separation of nanoparticles, specifically for the efficient recovery of EVs. By applying negative
625 pressure to the micropump, EV-containing solution is dragged through the ODEP operating
626 area within a double-sided tape microchannel, as shown in Fig. 5a. A strategically positioned
627 curved light pattern in the main flow channel aligns with the fluid's parabolic velocity
628 distribution, effectively enriching EVs in the light-spot region and improving recovery
629 efficiency through microfluidic recirculation (Fig. 5b). EVs, ranging in size from 60 to 250 nm,
630 experience a positive ODEP force (~23.5-97.7 fN with applied voltage of 20 Vpp at 20 kHz),
631 with the system achieving an impressive EV release efficiency of 99.8%, a recovery rate of
632 52.2 %, and a 272-fold concentration increase for a 27 pL sample volume. TEM images in Fig.
633 5c confirm the spherical and cup-shaped morphology of EVs before and after OET
634 manipulation, with non-EV nanoparticles being excluded due to their different dielectric

properties. This work demonstrates the successful integration of ODEP and microfluidics for efficient EV separation, holding significant potential for applications in early cancer diagnosis and targeted drug delivery[118].

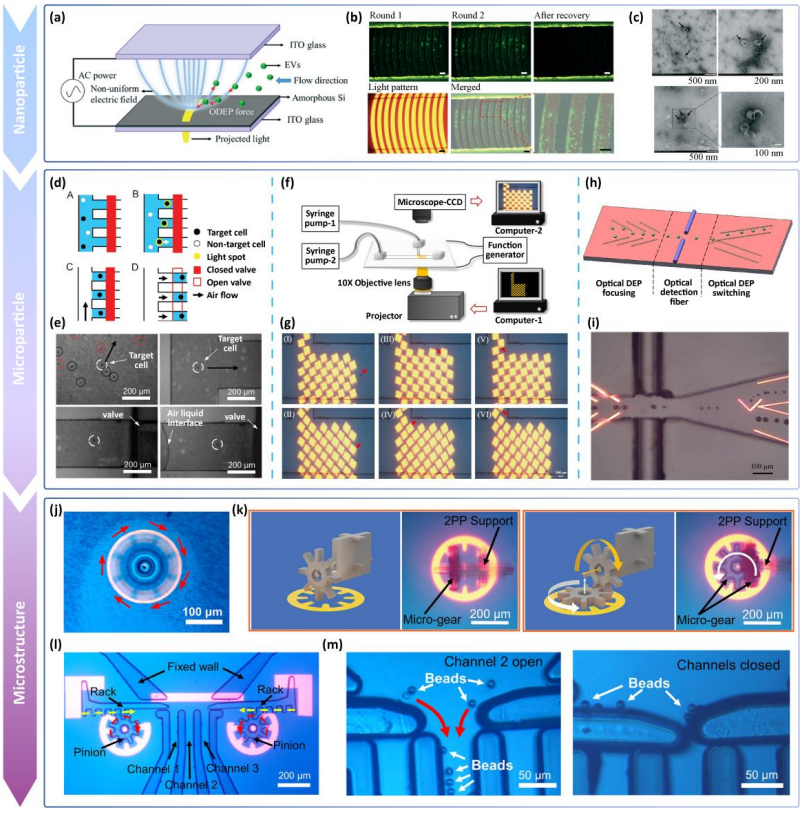

Fig. 5. OET manipulation of nanoparticles, microparticles, and microstructures. (a) Enrichment of EVs using ODEP force, where EVs experience a positive ODEP force. (b) TEM image of spherical EVs before OET manipulation. (c) TEM image of cup-shaped EVs after OET manipulation. (a and b and c) Reproduced from ref. 118 with permission from Royal Society of Chemistry, copyright 2021. (d) Extraction process of target cell in a microfluidic channel using OET. (e) Consecutive images showing target cells identified under brightfield from a population using a light beam. (d and e) Reproduced from ref. 177 with permission from Royal

Society of Chemistry, copyright 2013. (f) Overall experimental setup for cell separation. (g) Manipulation process for isolating cancer cell clusters in the main channel based on ODEP force. (f and g) Reproduced from ref. 150 with permission from Elsevier, copyright 2018. (h) Schematic of an optically induced flow cytometry chip used for particle counting and sorting. (i) Particles are successively separated by weaker and stronger virtual electrodes induced by different ODEP forces. (h and i) Reproduced from ref. 180 with permission from Elsevier, copyright 2008. (j) Changing the horizontal fluid field distribution by rotating micro-gears. (k) Changing the three-dimensional distribution of the fluid field by running a multiplanar micro-gear-train. Reproduced from ref. 193 with permission from Advanced materials, copyright 2025. (l) Schematic of the rack-and-pinion structure working in tandem. (m) Utilization of a micro-rack and pinion structure as a valve to control the movement of 10 μm diameter microbeads in the microfluidic channels. (j, l, and m) Reproduced from ref. 42 with permission from Nature, copyright 2021.

The integration of OET with microfluidic systems provides a powerful framework for sorting microscale objects, from biological cells to particle clusters, based on their intrinsic physical properties. The true advantage of this synergy lies in its remarkable versatility, enabling distinct modes of manipulation ranging from high-purity targeted isolation to continuous, label-free sorting and reconfigurable flow cytometry.

A primary application is high-purity cell sorting, where target cells are individually identified, isolated, and extracted from heterogeneous populations (Fig. 5d). This process typically involves identifying a target cell by its morphology or fluorescence (Step A) and using OET to capture and transport it to a dedicated collection channel (Step B). Subsequently, non-target sample is removed from the main channel, often by pneumatic flushing (Step C), before the isolated sample is extracted for downstream analysis (Step D)[177]. This capture-and-release methodology combines high-velocity fluidic transport with the precision of OET manipulation, ensuring exceptional purity in the extracted sample, which is critical for applications like the isolation of rare circulating tumor cells (CTCs) from blood (Fig. 5e). Beyond isolating single

675 cells, the integrated platform excels at the label-free sorting of cell clusters based on size. By
676 generating a dynamic array of light patterns within a microfluidic channel, OET can exert
677 tailored ODEP forces to controllably manipulate particle clusters (Fig. 5f). This all-optical
678 approach avoids the filter fouling and high shear forces characteristic of traditional mechanical
679 separation techniques, marking a significant improvement for applications such as cancer
680 diagnostics (Fig. 5g)[150]. Furthermore, the dynamic nature of OET enables the creation of
681 reconfigurable, optically-induced flow cytometry systems (Fig. 5h)[180]. In such a device, a
682 particle stream is first focused into a narrow line by negative ODEP forces from virtual
683 electrodes. As particles pass through an integrated optical fiber detection zone, their properties,
684 such as diameter, are analyzed. Based on this real-time analysis, the dynamic sorting zone is
685 activated to deflect specific particles into different microchannels. While challenges remain in
686 resolving particles with minimal size differences (< 3 μm), this method establishes an efficient
687 and scalable platform for high-throughput analysis and sorting, where the sorting criteria can
688 be reprogrammed on demand.
689 One of the key advantages of the OET technique is that the applied ODEP force is
690 proportional to the volume (or cube of the radius) of the manipulated object. Therefore,
691 integrating OET with channel-microfluidics enables precise manipulation, effective separation
692 and efficient analysis of biological targets across scales by exploiting volume/size-dependent
693 electrokinetic forces. Zhang *et al.* first exploited this principle to manipulate microrobot and
694 micromachines with sizes over 100 microns using OET, marking a significant milestone in
695 OET-microfluidic research[42]. OET-controlled micromachines extend beyond basic flow
696 channel actuation, enabling direct regulation of fluid velocity in targeted regions[42]. As
697 demonstrated in Fig. 5j, a micro-gear rotating at 360°/s alters the horizontal flow velocity and
698 direction, evidenced by the trajectories of adjacent 1 μm Ps beads. For simultaneous flow
699 control across different planes[193], multi-component micro-gear trains assembled via OET can
700 be used to create stable three-dimensional flow fields, as shown in Fig. 5k.
701 Fig. 5l shows a microfluidic structure with three parallel microchannels on top of an OET
702 bottom plate. This system can function as a variable control valve, using a micro-rack-and-

pinion mechanism to control the flow of a particulate suspension. By employing a dynamic light pattern to control the rotational motion of the pinion structure, the system allows for tandem control of the two micro-rack structures, enabling fluidic flow into any of the three micro-channels with a flow rate of up to 5 μL/min. Fig. 5m demonstrates the use of a micro-rack structure as a valve to control the movement of 10 μm diameter microbeads within the microfluidic channel. The direct control and manipulation of multiple microfluidic components to redirect fluid flow using OET represents a major advancement, which greatly expand the versatility and functionality of OET as a micro-assembly tool and may of useful for many micromanipulation and microfluidics related applications[194,195].

3.3. OET-Channel Microfluidics-based Biological Study

OET microfluidic integration techniques has broad applications in cell biology research, including cell kinetics analysis, electroporation, cell fusion, and cell lysis. Channeled microfluidic devices create a suitable micro-environment for biological samples, while OET technology offers low power density for non-invasive manipulation. This combination provides a safe and efficient approach for processing and analyzing delicate biological targets.

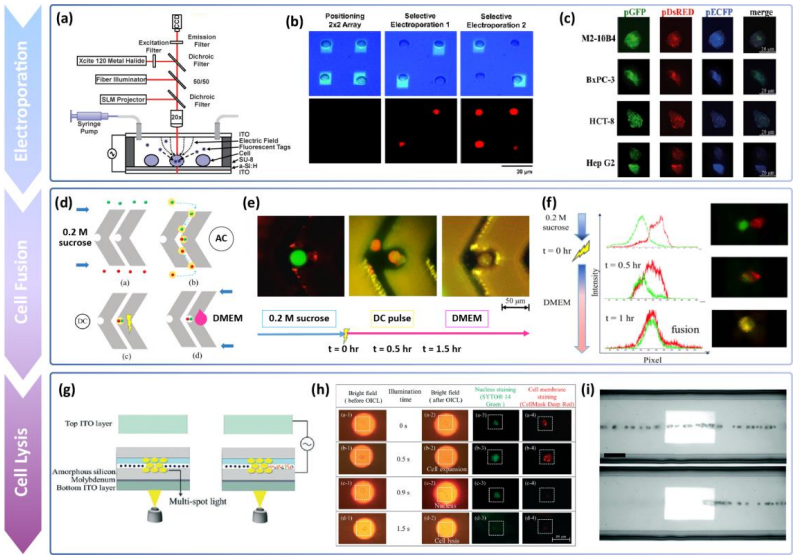

Fig. 6. Application of OET-microfluidic integration in biological research. (a) Experimental setup and mechanism for optically induced electroporation. The optical pattern concentrates the electric field on the cell, leading to selective single-cell electroporation. (b) Parallel electroporation of cells along the diagonal. (a and b) Reproduced from ref. 200 with permission from Royal Society of Chemistry, copyright 2009. (c) Transfection of plasmids carrying triple fluorescence into various cell types. Reproduced from ref. 149 with permission from Royal Society of Chemistry, copyright 2014. (d) Schematic diagram of optically induced ODEP and optically induced cell fusion. (e) Brightfield and fluorescence images showing cell fusion and the transformation into hybrid cells after 1.5 h incubation. (d and e) Reproduced from ref. 152 with permission from AIP Publishing, copyright 2018. (f) Fluorescence intensity distribution and fluorescence images of HeLa cells and A549 cells fused together using OET. Reproduced from ref. 151 with permission from Scientific Reports, copyright 2016. (g) Schematic diagram of optically induced cell lysis. (h) Relationship between cell membrane cleavage and light exposure time. (g and h) Reproduced from ref. 179 with permission from Royal Society of Chemistry, copyright 2014. (i) High-throughput cell lysis in microfluidic channels using ODEP force and acoustophoretic force. Reproduced from ref. 203 with permission from SPIE, copyright 2019.

The OET-channel microfluidics integration enables precise, selective electroporation at significantly lower voltages, improving cellular viability and throughput in biomedical applications[149,196]. Unlike conventional electroporation methods, which require high voltages and often result in irreversible cellular damage, the OET-microfluidic integrated technique precisely targets selected cells through dynamically controlled, light-induced AC electric fields[197-199]. This approach minimizes detrimental effects on adjacent cells and reduces thermal stress by employing a low optical power density (below 1 W/cm²). Additionally, electrode geometries and optical illumination patterns can be flexibly designed and modulated, facilitating parallel electroporation of multiple cells simultaneously while maintaining subcellular spatial control. Fig. 6a illustrates the underlying mechanism of selective

748 electroporation facilitated by optically patterned electric fields[200]. Targeted illumination
749 concentrates the electric field intensity precisely at the cell location, inducing transient
750 permeabilization of the cell membrane once the electric field surpasses the threshold value.
751 This allows controlled intracellular delivery of exogenous molecules while enabling subsequent
752 membrane recovery and preservation of cell viability. Experimental verification, as presented
753 in Fig. 6b, highlights the platform's capability to selectively electroporate individual cells
754 within a precisely arranged array. Cells initially manipulated using OET under a moderate field
755 strength (0.2 kV/cm) exhibited no membrane disruption. Subsequent application of a controlled
756 electroporation pulse (1.5 kV/cm, 100 kHz, 5 s) selectively permeabilized targeted cells, as
757 evidenced by propidium iodide uptake, while adjacent cells remained unaffected. Follow-up
758 studies employing various plasmids (pGFP, pDsRed, pECP) successfully demonstrated the
759 platform's capability to efficiently transfect diverse mammalian cell lines (Fig. 6c), including
760 mouse bone marrow stromal cells, human pancreatic cancer cells, colon cancer cells, and
761 hepatocytes. These outcomes underscore the advantages of the OET-microfluidic integrated
762 system in providing high-precision, minimally invasive electroporation for a wide range of
763 biotechnology and biomedical applications.

764 By establishing micro-traps within microchannels and using OET to capture individual
765 cells, precise and efficient cell fusion can be achieved. It provides an effective approach for
766 generating hybrid cells through the pairing and fusion of different cell types[151,152]. This method
767 utilizes OET to guide cells into a confined microfluidic trap, where they are held in place,
768 allowing for controlled pairing. Subsequently, an alternating electric field is applied, enabling
769 the mixing of cytoplasm across the cell membranes at the interface, thus facilitating fusion.
770 This technique holds significant promise for applications in monoclonal antibody production,
771 genetic engineering, regenerative medicine, immunology, and the creation of new cell lines. As
772 depicted in Fig. 6d, the OET microfluidic device guides A549 and Pan1 cells into specific
773 microfluidic channels, where they are first isolated based on differences in hydraulic pressure.
774 The cells are then manipulated using light patterns, bringing them into close contact for pairing
775 (Step a and b). An electrical pulse is applied to induce fusion, after which the fused cells are

776 cultured in a medium chamber to promote growth and further development (Step c and d)[152].
777 The setup ensures a controlled environment with temperature regulation, allowing for the
778 successful culture of hybrid cells after fusion. In this system, the OET device not only assists
779 in the precise handling and pairing of cells but also facilitates the photo-induced electrofusion,
780 resulting in the formation of hybrid cells. Notably, cell pairing is achieved through the pre-
781 fabricated microstructures[151], where an individual cell flows into the microstructure at a time,
782 ensuring that cells are paired efficiently while debris is washed away. The controlled flow rates
783 further enhance the accuracy of the pairing process. Fluorescence images shown in Fig. 6e
784 capture the fusion process, where hybrid cells become visible 1.5 hours after the application of
785 a DC pulse. The results demonstrate that the fusion of HeLa and A549 cells, as shown in Fig.
786 6f, is highly effective, with the fluorescence peaks of both cell types overlapping after an hour
787 of incubation, confirming successful fusion. This controlled microfluidic environment
788 minimizes disturbances during fusion and significantly enhances the yield of hybrid cells,
789 highlighting the efficiency and potential of the OET-microfluidic integrated device in cell
790 fusion and related applications.

791 The extraction of cell nuclei is an essential technique for applications such as disease
792 diagnosis, gene replication, and animal cloning[49,201,202]. An integrated system combining OET
793 with continuum microfluidics facilitates optically induced cell lysis (OICL) for the efficient
794 and automated extraction of cell nuclei. This system includes a micro-pump that controls the
795 flow of cell samples from the OICL module to the ODEP module, ensuring consistent
796 processing. In the cell lysis zone (Fig. 6g)[179], a digital projector generates multiple light spots
797 (75 μm in diameter), while an AC voltage applied to ITO glass substrates creates an strong
798 electric field that induces the desired transmembrane potential across the cell membrane. The
799 locally enhanced electric field near the virtual electrode disrupts the cell membranes in the
800 targeted region without affecting the nucleus. The intensity of the virtual electrode light is set
801 to 3.2 W/cm², which is sufficient to break the HEK293T cell membrane while keeping the
802 nucleus intact. Following lysis, cell debris, nuclei, and un-lysed cells pass through the ODEP
803 module, where a moving light bar applies a downward force using ODEP, facilitating the

separation of the components. Fig. 6h demonstrates the relationship between the duration of light exposure and cell membrane cleavage. At 0.5 seconds of exposure, the cells remain intact, as indicated by green and red fluorescence[179]. However, after 1.5 seconds of OICL exposure, both fluorescence signals vanish, indicating the completion of cell lysis. The system's lysis efficiency is further improved by integrating acoustic tweezers (AT)[203], where OET manipulates particles within a microfluidic channel made of SU8, and AT generates an acoustic radiation force that propels cells toward the pressure node at the center of the channel. Fig. 6i shows a red blood cell (RBC) undergoing continuous lysis as it passes through the illuminated region, demonstrating complete dissolution.

The integration of OET with channel-microfluidic systems enables a suite of high-precision cellular manipulation techniques for advanced biomedical applications. This platform can achieve targeted single-cell electroporation at reduced voltages with minimal thermal stress and facilitate efficient cell fusion through optically guided pairing. Furthermore, the technology enables high-throughput, automated cell nucleus extraction via optically induced lysis. In a demonstrated hybrid OET-acoustofluidic system[201], a cell lysis efficiency exceeding 99% is achieved for sample concentrations of 10^6 cells mL^{-1}. Operating at a continuous liquid flow rate of 3 μL/min, this performance translates to a processing throughput of thousands of cells per minute[203], confirming the platform's powerful capability for rapid, large-scale sample preparation.

At the system application level, biofouling represents a primary obstacle to long-term operational stability and analytical accuracy. The most effective solution lies in advanced surface engineering, specifically the application of anti-fouling coatings. Modifying the chip surface with materials such as polyethylene glycol (PEG) brushes or zwitterionic polymers creates a dense hydration layer, which effectively prevents the non-specific adsorption of proteins and cells via steric hindrance. Looking ahead, future intelligent systems may integrate active cleaning functions utilizing acoustic waves or localized electric fields to periodically dislodge adhered contaminants on demand. Overcoming biofouling through these passive and

active strategies is critical for ensuring the high reproducibility and reliability required for sensitive applications in diagnostics and long-term cell-based assays.

In summary, the integration of OET with channel microfluidics creates a robust platform for high-throughput manipulation in continuous flow, excelling in applications such as cell sorting, lysis, and electroporation. However, continuous-flow systems face inherent limitations when discrete, isolated microenvironments are required for extended single-cell culture or multi-step chemical reactions. To address these needs, the field has evolved toward droplet-based architectures. In the following section, we discuss the integration of OET with DMF, which offers precise control over discrete droplets to facilitate complex, multi-step biochemical assays.

IV. OET-Digital Microfluidics Integration

In addition to the integration with channel microfluidics, OET can also be integrated with DMF, which is based on electrowetting-on-dielectric (EWOD) effect to manipulate droplets[204-206] for many unique applications in the microfluidic field. The combination of OET with DMF provides a useful tool for research on biochemistry and biomedical engineering.

4.1 Integration and Working Mechanism

As shown in Fig. 7a, the first-generation of OET-DMF integrated device features a layered structure: EWOD electrodes and a dedicated central OET electrode are integrated on the top glass substrate, while a photoconductive amorphous silicon layer is deposited on the bottom substrate[188]. This design physically separates the OET and EWOD regions to prevent dielectric interference, though it sacrifices operational continuity. The EWOD electrodes initially transport cell-containing droplets into the OET region (Fig. 7b). The OET generates a lateral electric field gradient through light patterning to enable cell sorting (Fig. 7c). Finally, droplet splitting creates independent microenvironments for single-cell isolation (Fig. 7d).

To address the spatial segregation limitations of the first-generation device, a second-generation lateral-field OET (LOET) device was introduced (Fig. 7e)[207]. This design integrates

interdigitated electrodes on a single substrate, eliminating the physical boundaries between the OET and DMF regions. As shown in Fig. 7f, LOET electrodes share the same substrate as the EWOD electrodes, requiring only a photoconductive layer and hydrophobic coating on the bottom substrate. This design simplifies fabrication and broadens the operational range.

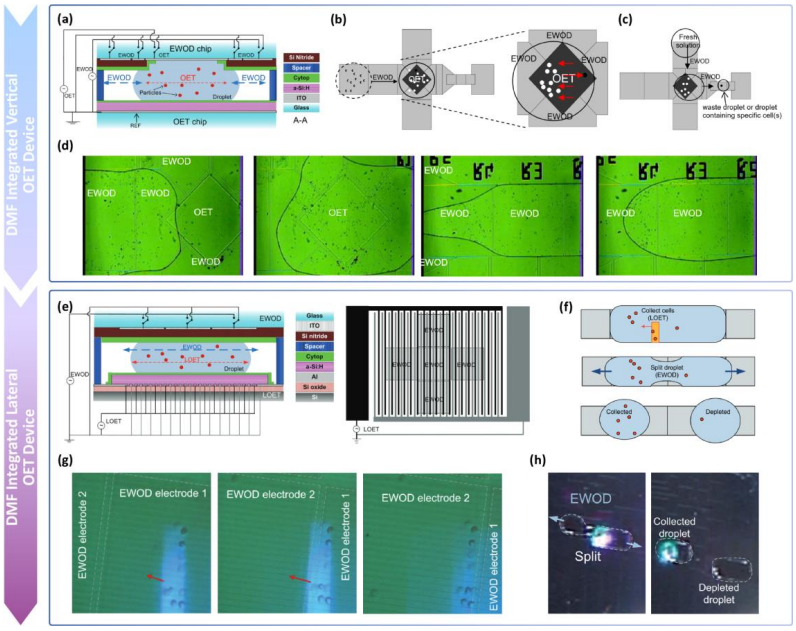

Fig. 7. Integration of OET with DMF. (a) Layered structure of the first-generation integrated device, highlighting the spatial separation of OET and EWOD electrodes. (b) Close-up image of the top substrate, showing the photoconductive layer in the OET region and the distribution of the hydrophobic coating. (c) Schematic of droplet transport into the OET region via EWOD actuation. (d) Droplet splitting process to create target-cell-enriched microenvironments. (a-d) Reproduced from ref. 208 with permission from IEEE, copyright 2006 (e) Cross-sectional view of the second-generation LOET design, enabling co-planar OET-DMF operation. (f) Co-planar electrode layout, simplifying fabrication and expanding the operational range. (g) Light-induced electric field gradient used for long-range cell manipulation. (h) Workflow consisting of droplet positioning, sorting, and splitting. (e-h) Reproduced from ref. 207 with permission from Royal Society of Chemistry, copyright 2009.

874

875 **4.2 Applications**

876 The vertical-field OET (VOET) can be applied to specific regions within a DMF chip to
877 manipulate particles or cells inside droplets[208]. The two functional regions are independent and
878 integrated within a sophisticated design, as shown in Fig 7a. However, due to the separation of
879 OET and EWOD functions, particle arrangements achieved by OET are difficult to maintain
880 when fluids are moved around, such as during droplet splitting. Moreover, the strict functional
881 separation significantly reduces the advantages of EWOD in high-throughput droplet
882 operations.

883 In contrast, LOET is more suitable for integration with DMF[207]. The parallel arrangement
884 of OET electrodes eliminates the need for strict functional zoning. OET-based tasks such as
885 particle manipulation and cell sorting can be performed anywhere on the chip within the span
886 of the interdigitated electrodes (Fig. 7g). Meanwhile, droplet movement, mixing, and splitting
887 can be achieved simultaneously (Fig. 7h). The high-throughput capabilities of DMF in droplet
888 handling are preserved, and the combined functions facilitate applications such as running
889 biochemical assays, medium exchange, enrichment of cell secretions (e.g., proteins, exosomes),
890 and high-throughput biochemical analysis. The integration of OET and DMF marks a
891 significant advancement in micro/nano manipulation, transitioning from single-modality
892 operations to multifunctional systems. With further advancements in electrode design, material
893 engineering, and intelligent control systems, this hybrid platform is poised to find widespread
894 applications in precision medicine, synthetic biology, and beyond[209-213].

895 Overall, the OET-DMF integration successfully combines the flexibility of optical
896 manipulation with the programmable droplet handling using EWOD. While this hybrid
897 approach significantly enhances bioassay capabilities, traditional DMF relies on fixed,
898 prefabricated electrode arrays, which can limit the spatial resolution and reconfigurability of
899 droplet trajectories. To overcome the constraints of fixed electrodes, OEW technology has
900 emerged as a solution. As detailed in the next section, OEW utilizes photoconductive layers to

create "virtual electrodes" anywhere on the surface, enabling light-driven, featureless droplet manipulation.

V. OET-Optoelectrowetting Integration

In this section, we will provide an overview of the integration of OET with OEW, discuss the working principle of OEW, and explore its applications in microdroplet manipulation and biochemical analysis.

5.1. Integration and Working Mechanism

The OEW is a liquid manipulation technology that allows precise control over the motion of individual microdroplets. Electrowetting requires the droplet to be in contact with two regions of different voltage. In conventional approaches, this is achieved through multiple physical electrodes. In OEW, light induced virtual electrodes are used to selectively change the voltage around a specific area, causing the contact angle in the vicinity to change. This change in contact angle translates into droplet motion[214]. In other words, the light-induced "virtual electrodes" selectively convert hydrophobic surfaces to hydrophilic ones, effectively attracting nearby droplets[215-220]. When integrated with OET, OEW enables the combined manipulation of droplets and intra-droplet particles through the application of light-controlled electric fields[221]. This integration offers several benefits, such as dynamic programmability, high precision, low contamination, and versatility. As a result, it provides a powerful platform for advanced biomedical research, including single-cell analysis and organ microarrays, as well as high-throughput chemical synthesis. This innovative design represents a significant step forward in the development of next-generation intelligent microfluidic systems.

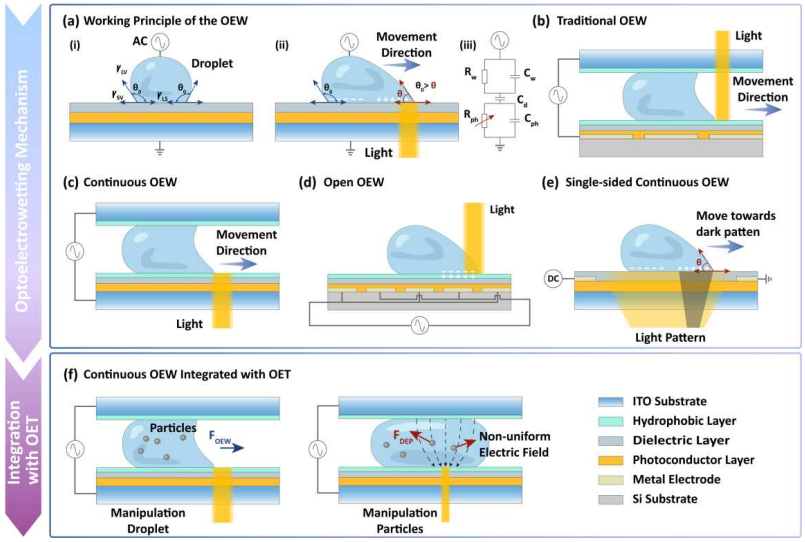

Fig. 8. OEW device mechanisms. (a) Working principle of OEW. (b) Droplet actuation on a traditional OEW device. (c) COEW device that enables flexible positioning of droplets on a featureless photoconductive surface. (d) Schematic of OOEW. (e) Schematic of SCOEW, which facilitates easy integration with portable testing equipment. (f) Integration of OEW and OET for the manipulation of droplets and particles on a chip. The object to be manipulated is selected by changing the voltage frequency.

The OEW device, which consists of a bottom substrate and top substrate, with the top substrate typically being a transparent glass coated with indium ITO, while the bottom substrate, similar to an OET device, includes an additional dielectric layer and a hydrophobic coating. Optical addressing on the photoconductive surfaces of the OEW induces the electrowetting effect. The system setup of the OEW is similar to that of OET and supports dynamic droplet manipulation without relying on complex pumps or valves. The OEW chip can be modeled as having three electrical impedances corresponding to the droplet, dielectric, and photoconductor layers, connected in series. To actuate the droplet, an AC voltage is applied between the droplet and the bottom electrode.

In the absence of light (i.e., in the dark state), the droplet remains close to its initial contact angle on the solid surface because most of the voltage drop occurs across the photoconductor layer, where electrical impedance is the dominant factor. The voltage drop across the dielectric layer is negligible, and the contact angle remains virtually unchanged (Fig. 8a i). When light is applied to the photoconductive layer after passing through the transparent electrode, excess electron-hole pairs are generated, significantly increasing the local conductivity in the illuminated region. As a result, the contact angle of the droplet decreases due to electro-wetting-on-dielectric effect (Fig. 8a ii)[222]. Applying a potential between the droplet and the solid electrode redistributes the charge, altering the surface tension at the liquid-solid interface. The repulsive force of like charges reduces the work by expanding the surface area. The droplet moves to the region of higher partial pressure in the dielectric layer. The contact angle (θ) of a droplet can be mathematically estimated using the Young-Lippmann equation[222-224]:

$$\cos\theta = \cos\theta_0 + \frac{c_d(\Delta V)^2}{2\gamma_{LG}} \quad (8)$$

Where，θ_0 is the initial contact angle of a droplet at zero applied potential, γ_{LG} is the surface tension between two immiscible fluids (i.e., the droplet and its surrounding medium), $c_d$is the capacitance per unit area of the dielectric layer, and ΔV is the voltage drop across the dielectric capacitor.

The traditional OEW device manipulates droplets that are confined between two parallel substrates (Fig. 8b). The top substrate features hydrophobically coated electrodes, while the bottom contains both grid and regular electrodes, with an a-Si:H layer sandwiched between them. When light strikes the droplet's edge, the conductivity of the α-Si layer increases drastically, causing the voltage drop to primarily occur across the SiO_2 dielectric layer in the illuminated region[222,225]. This creates a localized electrical wetting effect that alters the droplet's contact angle, moving it toward the light-illuminated area. While traditional OEW devices solve complex wiring issues common in DMF systems, they still rely on photolithographic patterning of the photoconductive layer, complicating the fabrication process. In contrast, the continuous OEW (COEW) device offers a simpler fabrication process and greater flexibility in droplet manipulation (Fig. 8c)[226]. This version retains the sandwich structure but uses continuous

deposition for both the photoconductive and electrode layers. The top substrate mirrors the conventional OEW design, while the bottom features sequential layers, including hydrophobic, dielectric, and photoconductive layers, eliminating the need for photolithography. This configuration enables flexible droplet positioning on the photoconductive surface, supporting continuous droplet transport. To optimize operation, Atomic Layer Deposition (ALD) is used to apply an Al_2O_3 dielectric layer, enhancing the dielectric constant and reducing the AC bias to 16 Vpp[227]. The closed structure prevents microdroplet evaporation, but integration with external systems remains challenging, limiting flexibility. To overcome integration issues of closed systems, open OEW (OOEW) devices were introduced. These devices retain the same functional layers but adopt an open configuration. The patterned electrodes are covered by a hydrophobically coated dielectric layer, sitting on a photoconductive a-Si layer. Applying an AC bias to the electrodes modifies the electrical impedance in the photoconductive layer[228-230], resulting in voltage drops across the dielectric layer in the illuminated region. This lowers the droplet's contact angle, enabling optical actuation. However, OOEW devices still require patterned electrodes, and the minimum droplet size manipulable is constrained by the dimensions of the electrode array.

Furthermore, single-sided continuous OEW (SCOEW) devices have been developed, utilizing organic photoconductors such as TiOPc. This innovation reduces fabrication costs and enhances integration with microfluidic components[40,47,220,231]. Fig. 8e demonstrates the SCOEW device's capability for continuous droplet manipulation using optical patterning on open, featureless photoconductive surfaces. This single-sided open configuration offers a flexible interface, allowing integration with other microfluidic components, such as sample reservoirs, microchannels, and portable systems. Dynamic and reconfigurable optical patterns enable continuous droplet transport, splitting, merging, and mixing, overcoming the size constraints of pixelated electrodes. However, as in any unsealed device containing small volume of liquid, fluid evaporation remains a challenge. In addition, the manipulated droplet volumes are typically much larger (in the microliter range).

As microfluidic and micro total analysis system (μTAS) technologies evolve, integrating multiple functions onto microfluidic chips is creating versatile platforms for biological and chemical applications. The OET-OEW integrated devices have been demonstrated for on-chip sample concentration, purification, and single-particle encapsulation. Fig. 8f shows a device that combines OET and OEW, allowing users to manipulate liquid droplets using OEW and individual particles within those droplets using OET by simply adjusting electrical frequencies. A fundamental challenge in achieving a monolithic OET-OEW integration lies in the divergent frequency requirements dictated by the system's interfacial impedance network. The hybrid platform operates essentially as an optically modulated voltage divider. At low AC frequencies (typically < 10 kHz), the capacitive reactance of the insulating dielectric and hydrophobic layers dominates the circuit. Upon optical illumination, the photoconductive layer's impedance drops, localizing the applied potential predominantly across the dielectric layer. This low-frequency regime maximizes the electrostatic energy stored in the capacitor, driving OEW droplet actuation via the Lippmann-Young mechanism[218]. Conversely, OET necessitates high-frequency actuation (typically > 10 kHz) to bypass the EDL and the dielectric capacitance. At these frequencies, the voltage drop is effectively transferred to the bulk fluidic layer, generating the required spatial electric field gradients ($|E|^2$) for ODEP particle trapping. To resolve this intrinsic impedance mismatch and prevent mechanism interference, integrated platforms employ frequency-selective time-division multiplexing[41,232]. By dynamically switching the AC bias frequency, the system can selectively route the electrodynamic power to either the solid-liquid interface or the bulk fluid. This temporal modulation strategy enables the seamless, sequential execution of macro-scale droplet routing (OEW phase) and micro-scale ODEP manipulation (OET phase) within the exact same spatial footprint. OET enhances OEW's capabilities, especially in fine droplet control and complex particle manipulation, addressing OEW's limitations in handling internal materials and objects within droplets. This unified platform facilitates seamless control of both droplets and particles, offering easy switching between the two modes by adjusting frequency. Unlike traditional systems that rely on complex lithography and fixed electrode setups, this platform eliminates the need for lithography,

simplifying fabrication and enabling manipulation across the entire device surface. The use of patterned light to define electrodes further allows precise 2D control of individual particles, making it highly flexible and accurate. It also enables the selection and encapsulation of individual cells, making it an ideal solution for biological and chemical applications, particularly those requiring high resolution, low cost, and reconfigurability.

While dynamic frequency modulation successfully resolves the electrical impedance conflicts, the actual physical execution of reversible droplet routing remains fundamentally dependent on the physicochemical integrity of the solid-liquid interface. Beyond the electrical impedance network, a critical boundary condition for the sustained operation of OEW and digital microfluidic platforms is the thermodynamic stability of the solid-liquid interface[222]. Sustained OEW operation relies heavily on the thermodynamic stability of the solid-liquid interface. In complex biological fluids, non-specific protein adsorption onto the hydrophobic layer alters the local surface free energy[233]. This biofouling induces severe contact angle hysteresis, effectively 'pinning' the droplet and drastically increasing the drag resistance against optical actuation. This protein adsorption induces severe contact angle hysteresis, effectively 'pinning' the droplet's three-phase contact line and dramatically increasing the threshold viscous drag required for actuation.

To mitigate this interfacial degradation and maintain the reversibility of the electrowetting phenomenon, advanced surface passivation strategies are strictly required. Currently, the deposition of amorphous fluoropolymer coatings (e.g., Teflon AF or Cytop) serves as the primary physical barrier, establishing an initially high static contact angle (> 110°) to minimize the baseline surface energy. Furthermore, this static hydrophobicity is dynamically reinforced by supplementing the aqueous phase with non-ionic triblock copolymer surfactants (such as Pluronic F127)[233]. These surfactants dynamically self-assemble at the liquid-solid interface, creating a steric hydration layer that physically repels protein deposition. This dual-layer approach—combining static fluoropolymer hydrophobicity with dynamic steric repulsion—is essential for preserving the low-friction boundary conditions necessary for seamless, long-term optical droplet routing without cross-contamination.

5.2. Flexible Droplet Manipulation based on OEW

The concept of OEW as a mechanism for light-driven droplet actuation was first introduced by Ming C. Wu et al[218]. OEW combines optical manipulation techniques with the electro-wetting effect, using light to modify the local charge distribution on the electrode surface, thereby enabling precise control over droplet motion. The use of a tunable light field to regulate the droplet's dynamic behavior allows OEW techniques to move beyond the limitations of static control, enabling dynamic manipulation of droplets. Since its inception, OEW has shown significant potential for a range of applications in the fields of biomedical research (e.g., droplet microreactors[234-238], lab-on-a-chip[224,239-241], cell manipulation), consumer electronics, materials science[223], and more.

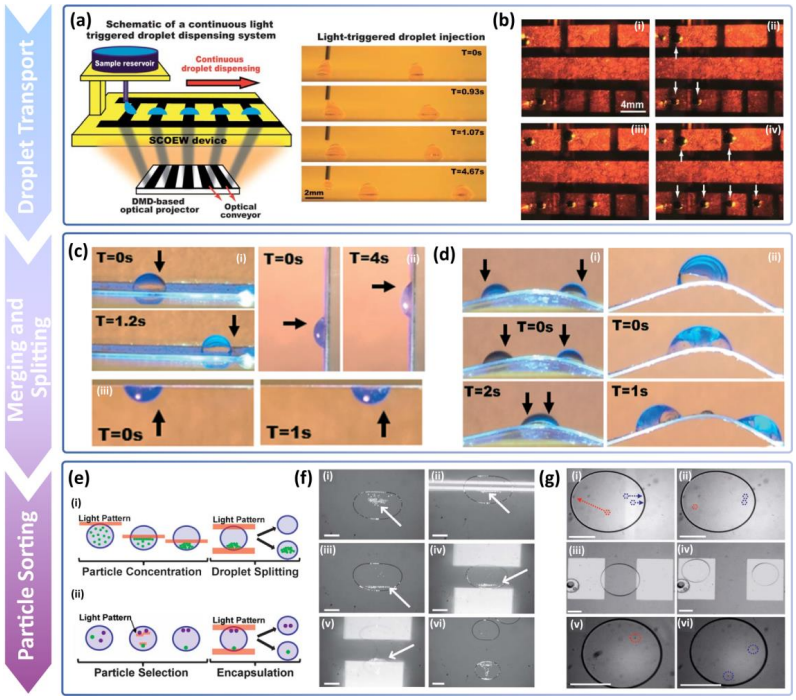

Fig. 9. OEW integrates with other components for flexible droplet manipulation. (a) Schematic of the external sample reservoir for OEW-integrated light-triggered droplet injection. (b) Two

external reservoirs enable continuous, parallel injection and delivery. (a and b) Reproduced from ref. 231 with permission from Royal Society of Chemistry, copyright 2010. (c) Light-driven 3D droplet manipulation on flat, vertical, and inverted surfaces. (d) Droplet merging and splitting on curved surfaces. (c and d) Reproduced from ref. 220 with permission from Royal Society of Chemistry, copyright 2016. (e) Integration of OET with OEW to enable continuous particle concentration and single-cell selection and encapsulation. (f) Experimental demonstration of particle concentration. (g) Experimental demonstration of single-cell selection. (e-g) Reproduced from ref. 221 with permission from Royal Society of Chemistry, copyright 2011.

SCOEW devices can achieve electrowetting using optical patterns on feature-free photoconductive surfaces (Fig. 9a)[231]. The SCOEW system integrates an open chamber structure with a sample reservoir, which generates microdroplets at equal intervals on the continuous photoconductive layer. Fig. 9b demonstrates the sequential injection of 2.5 μL droplets into the SCOEW chamber, with parallel injections from two external reservoirs. This setup allows continuous droplet positioning across the 2D surface, overcoming size limitations imposed by electrode pixelation. The system enables on-chip sample generation and delivery, suitable for downstream analysis and high-throughput droplet detection. Fig. 9c showcases the phototriggered, continuous injection of droplets from two reservoirs with volumes of 1.8 μL (top conveyor) and 0.9 μL (bottom conveyor), transported by dark-colored bar conveyors. This lateral-field-driven wetting mechanism operates at low light intensities, making it compatible with portable LCD displays without additional optical components.

High-throughput droplet transport facilitates advanced droplet manipulation. A flexible SCOEW device has been developed that uses titanium dioxide phthalocyanine (TiOPc) for light-driven 3D droplet manipulation. Fig. 9d shows continuous droplet transport on various 3D topographies—flat (φ=0°), vertical (φ=90°), and inverted (φ=180°), with gravity influencing the motion differently[220]. Droplet merging and splitting are crucial for managing biological or biochemical concentrations. Fig. 9e shows droplet merging on curved SCOEW

surfaces, where two droplets are driven to merge at the peak position. Droplet splitting is achieved by stretching a 6 μL droplet on a curved substrate under a 150 V/mm electric field, causing the droplet to divide due to the combined effects of OEW and gravity. This approach highlights the feasibility of droplet manipulation on flexbile substrates, paving the way for application scenieros that flexible devices or interfaces are needed[221]. However, challenges remain to scale the system down to work with picoliter droplets.

The OET-OEW integration enables the simultaneous manipulation of the droplet and the particles contained within it[221]. In this case, OET is used to transfer particles (or cells) within droplets and OEW is used to manipulate droplets, as shown in Fig.9e-g. The OET-OEW integrated device is normally used for for on-chip sample concentration and purification. Particles are concentrated at one end of the droplet using parallel light bar patterns, and OEW splits the droplet into two—one with concentrated particles and the other empty—effectively doubling the sample's concentration and purity. Iterative cycling through this process exponentially increases particle concentration by splitting the droplet with each cycle. Unlike DMF systems, where electrode size determines the smallest droplet size manipulable, the electrode size in this integrated device is governed by the light pattern size, allowing manipulation of droplets of various diameters. The smallest light pattern size is limited by the diffraction limit or photoconductive material's diffusion length, typically around 100 nm. Since diffraction limited spot sizes are usually larger, that is often the limiting condition. Traditional single-cell encapsulation methods rely on statistical approaches, generating a large number of droplets, but cannot select individual cells for encapsulation. Fig. 9g shows the selection of a single HeLa cell from a group of three. The selected cell is moved to one end of the droplet using OET (16 Vppk, 10 kHz), while the remaining cells are directed to the other end. Positive ODEP forces move the cells, while negative ODEP forces act on polystyrene beads. Using OEW (32 Vppk, 200 kHz), the droplet is split into two 75 nL droplets: one with the selected cell and the other with the remaining two cells. The OEW enables light-driven manipulation of droplets on featureless photoconductive surfaces, eliminating the need of physical electrodes as observed for DMF technology. This platform achieves gravity-independent droplet transport

across complex 3D topographies (0–180° inclination) and supports advanced operations like merging/splitting, while OET-OEW integrated systems permit simultaneous control of both droplets and encapsulated particles/cells. Critically, the synergy of optoelectronic forces enables high-precision, on-demand single-cell encapsulation through on demand cell manipulation and droplet splitting (~75 nL volumes), overcoming limitations of statistical encapsulation methods such as water-in-oil droplet microfluidics[242].

5.3. OEW-based Biochemical Analysis

In addition to the OET-OEW integrated device, microfluidic systems based on OEW chip can also be applied for a wide range of biochemical applications[243]. On these chips, discrete droplets containing biological or chemical samples can be manipulated individually or subjected to automated small-scale fluidic operations such as droplet injection, transport, separation, merging, sorting, and quantitative analysis[215-217,222,225].

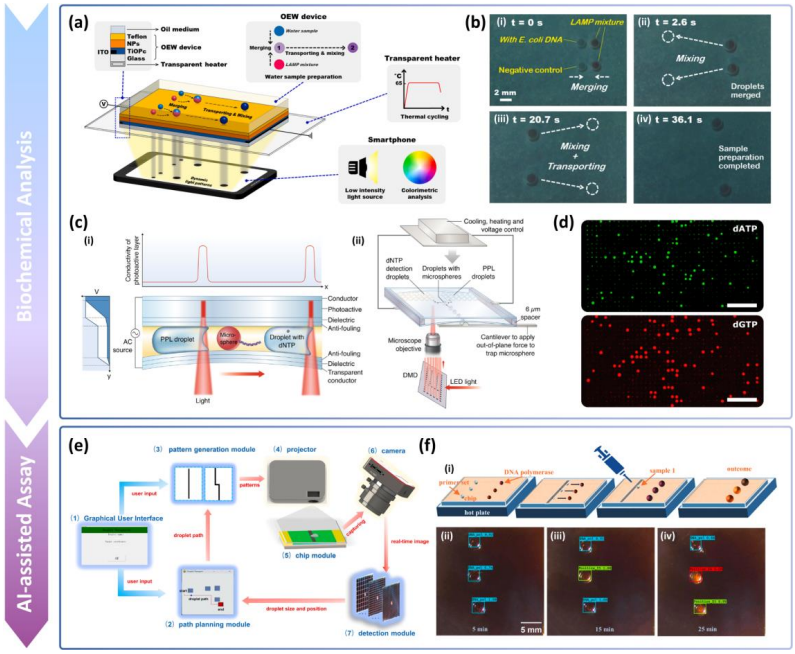

Fig. 10. OEW-based biochemical analysis and detection. (a) OEW platform for portable LAMP testing. (b) E. coli samples on-chip using freshwater droplets of E. coli DNA and LAMP mixture droplets. (a and b) Reproduced from ref. 239 with permission from Elsevier, copyright 2022. (c) OEW sequencing platform with integrated temperature/voltage control. (d) Fluorescence images of portions of microdroplet arrays in the dATP and dGTP channels. Scale bars are 100 μm. (c and d) Reproduced from ref. 235 with permission from Oxford University Press, copyright 2020. (e) AI modularized universal droplet-based SCOEW chip processing system. (f) AI-LAMP assay for SCOEW with parallel testing of three samples. (e and f) Reproduced from ref. 47 with permission from Elsevier, copyright 2024.

The integration of OEW with a transparent heater and a smartphone, named lab-on-a-smartphone (LOS), enables a portable loop-mediated isothermal amplification (LAMP) system for on-site water quality testing (Fig. 10a)[239]. The OEW device facilitates on-chip LAMP mixing and water sample preparation by manipulating droplets using a low-intensity light pattern projected from the smartphone below. A transparent heater maintains the isothermal condition at 65°C for nucleic acid amplification during LAMP assays. Additionally, the smartphone acts as a portable colorimetric analyzer during the LAMP reaction, projecting dynamic light patterns onto the photoconductive surface of the OEW device. This eliminates the need for additional equipment—its display serves as the light source, while the smartphone's camera captures digital images of the water sample to calculate RGB values, enabling quantitative analysis of color changes over time. Fig. 10b demonstrates the successful processing of an on-chip E. coli sample using the OEW device, where two droplets were fused, transported, and mixed via a dynamic optical pattern from the smartphone. The OEW system offers direct on-chip readout of multiple droplets, each carrying important information, addressing limitations seen in single-cell sequencing technologies, which struggle with short-read platforms' difficulty in sequencing homopolymers and repetitive motifs, as well as long-read platforms' low throughput.

The OEW device was constructed as an optical electrowetting sequencing platform for stepwise release, capture and detection of deoxyribonucleotide triphosphate (dNTPs) in microdroplets of individual DNA molecules (Fig. 10c)[235]. Each microdroplet acts as a reaction vessel for detecting dNTPs based on fluorescence signals. DNA-bound microspheres are combined with volume-matched droplets containing dNTP detection reagents, which are then temperature cycled for the dNTP detection reaction. Droplet arrays are imaged using a fluorescence microscope. Fig. 10d displays images of 532 nm (dATP) and 655 nm (dGTP) fluorophores, with the dNTP content determined by fluorescence intensity in each channel relative to the entire droplet population. However, the OEW chips face limitations due to the physical constraints of microfluidic channels or operators manually locating droplets and planning their movement paths, leading to uncontrolled droplet flow and potential contamination. Recent advancements in AI-based intelligent droplet control systems address these challenges[47,234,239-241]. These systems use target detection algorithms to recognize droplet characteristics in real time, providing trajectory and ID information through a tracking algorithm to efficiently track droplet arrays. This enables automatic parallel control of droplet motion and fusion, facilitating the arrangement and relocation of disordered droplet arrays.

The development of an OEW droplet control system integrated with AI is advancing rapidly (Fig. 10e)[47]. The system comprises modules for droplet driving, detection, separation, and path planning. The user selects the driving mode and inputs preset parameters via a graphic user interface, which are sent to the path planning and pattern generation modules. The generated pattern is projected onto the chip, driving the droplets. A camera captures real-time images of the chip, transmitting them to the target detection module for droplet detection and information updates, which are fed back to the path planning module for further control. Fig. 10f demonstrates an AI-assisted LAMP assay on the OEW system, testing three samples in parallel. Primer sets and DNA polymerase were dispensed using a syringe pump, and the droplets merged to form a volume of 8 μL, requiring automatic adjustment of the pattern line width. The system automatically detects and merges target droplets based on their color, efficiently discriminating between positive and negative samples and estimating the initial

DNA concentration without colorimetric or fluorescence analysis. The integration of microdroplet analysis and AI highlights the feasibility of using OEW systems for water quality testing, molecular detection, and colorimetric reactions[239-241]. The integrated OEW platform can achieve automated, field-deployable biochemical analysis through light-driven droplet operation. This method combines smartphone-based control with photoconductive surfaces for portable LAMP detection, while the droplets consists of samples and reagents allow for single-molecule sequencing through fluorescently encoded dNTP detection. Crucially, the integration of OEW with AI-driven vision systems overcomes the limitations of manual operation, achieving autonomous imgaging recognition, droplet tracking and parallel processing that utilize molecular diagnosis for environmental monitoring and public health management.

To conclude, OET-OEW integration represents a versatile paradigm for handling both droplets and encapsulated particles on a single platform, utilizing AI-driven control to achieve high automation. The maturation of these technologies, from channel-based sorting to flexible droplet manipulation, has laid a solid foundation for transitioning from academic prototypes to industrial products. In the subsequent section, we examine the current landscape of commercialization, highlighting how these integrated optofluidic systems are being translated into standardized tools for the biopharmaceutical and clinical sectors.

VI. Commercialization

Driven by growing demand for OET-enabled solutions, significant industrial efforts have been made to commercialize the technology, especially for biopharmaceutical and fundamental research. A notable example for a basic research platform is the OptoBot® 500, an advanced desktop OET platform developed by Optoseeker Biotechnology (Shenzhen) Co., Ltd[244]. This system utilizes DMD projection technology to achieve precise spatiotemporal control of micro-/nanoscale entities—including metallic particles, dielectric microbeads, nanomaterials, droplets, micromachines and living cells. The OptoBot® 500 is engineered for versatility, integrating a fully functional OET actuation module, high-precision spatial light modulation, stable LED

illumination, ultra-high-resolution imaging capabilities, and customizable graphical interfaces. These features make it a powerful tool for applications in single-cell manipulation, droplet-based microfluidics, and nanoscale assembly. With the OptoBot® 500 system, users can realize customized functions through open ports, such as AI-based target recognition, multi-target path planning, adaptive light pattern generation and other flexible modules[50]. Coupled with OptoMind® 500 software, which allows for real-time pattern optimization and automated workflow management, the platform significantly enhances experimental throughput and reproducibility, benefiting academic OET/OEW research and industrial R&D in the life sciences[193,245].

Fig. 11. Commercialization of microfluidic OET technology. (a) OptoBot® 500 Optoelectronic Tweezer System, featuring the device and micro-patterns created from microparticles. (b) Beacon system for cell screening and selection, with a photograph of the system. The samples are loaded onto a proprietary OET-microfluidic chip, shown on the right. Reproduced from ref. 249 with permission from IEEE, copyright 2019. (c) Workflow for cell manipulation, analysis, and recovery using the Beacon system. Reproduced from ref. 254 with permission from Nature,

copyright 2018. (d) Illustration depicting a cross-section of the oEWOD chip. (e) A still image from a video showing the real-time droplet filter function on the platform, with annotations. (f) A stitched image showing 12,932 aqueous droplets arrayed across a section of the chip after loading and filtering based on size (100 μm diameter). (d-f) Reproduced from ref. 236 with permission from Royal Society of Chemistry, copyright 2024.

In the field of biotechnology, Ming Wu, the pioneer of OET technology, co-founded Berkeley Lights Inc. in 2011 with Igor Khandros and William Davidow[246]. Acquired by Bruker in 2023, this California-based company has significantly advanced the commercialization of fully automated OET platforms for high-throughput functional screening of single cells. Key applications include antibody discovery, cell line engineering, cell therapy development, and synthetic biology. The flagship Beacon platform[247], now part of Bruker's portfolio[248], integrates OET with a microfluidic chip featuring up to 20,000 NanoPen chambers—nanoliter-scale microenvironments interconnected by microfluidic channels for precise manipulation of cells, beads, and reagents (Fig. 11a & b)[249]. These NanoPen (ranging from 250 pL to 2 nL in volume) enable rapid phenotypic profiling of individual cells by isolating them from bulk populations while maintaining spatial control[250-253]. A typical workflow (Fig. 11c) on the Beacon platform combines OET-driven cell positioning with multiplexed functional assays[254]. Cells are loaded onto OptoSelect Chips and optically guided into NanoPens using light-induced ODEP. After clonal expansion, reagents are introduced to assess secreted proteins, surface markers, or metabolic activities. High-performing clones are then isolated for downstream genomic analysis or therapeutic development. This closed-loop system directly links cellular phenotypes to genotypes, streamlining the hit-to-lead selection process. For example, while traditional hybridoma workflows take 2–3 months to identify therapeutic antibodies, the Beacon platform accelerates this to days by screening single B cells. Its scalability and reagent efficiency also reduce costs and improve success rates in cell therapy pipelines.

Commercial implementation of this technology is exemplified by the Envisia platform from Lightcast Discovery Ltd., which enables highly multiplexed single-cell assays within

picoliter-scale droplets (Fig. 11d-f)[236]. The system leverages OEW to precisely manipulate these droplets, which function as independent biochemical microreactors. This optical control allows for high-speed droplet transport at 100–200 μm/s, facilitating essential assay steps such as splitting, merging, and sorting[236]. While the platform can generate approximately 660 droplets per minute, its operational throughput for targeted screening and sorting is approximately 120 droplets per minute. By integrating high-density droplet generation with programmable, parallel optical control, this technology provides a scalable pathway for complex cell profiling, with a roadmap to process over 100,000 single-cell assays on a single cartridge.

Despite current commercial progress, the broader integration of OET-based platforms into standard biotechnological workflows is constrained by several fundamental and technical bottlenecks. First, the economic scaling of instrumentation and high-performance photoconductive consumables remains unfavorable for decentralized academic or clinical settings compared to passive microfluidic architectures. Second, a definitive performance trade-off exists between OET's high spatial precision and its total operational throughput; the serial or semi-parallel nature of OET manipulation typically results in lower cell-processing rates compared to the continuous-flow regime of fluorescence-activated cell sorting (FACS)[255], particularly when sample populations exceed $> 10^7$ events. Furthermore, the electrodynamic stability of the photoconductor-liquid interface remains a challenge in high-conductivity physiological media ($\sigma > 1$ S/m). In such regimes, significant Maxwell-Wagner polarization and the formation of an EDL at the electrode surface leads to substantial potential drops across the interface, thereby attenuating the effective ODEP force acting on the target bioparticles. Finally, maintaining a stable interfacial energy to prevent non-specific biofouling during extended culture periods necessitates sophisticated surface functionalization, which introduces additional complexity to the device's boundary conditions and fabrication process[256].

Overall, OET-driven platforms have become transformative tools in immune-oncology, antibody discovery, stem cell engineering, and regenerative medicine. Their ability to precisely

manipulate and analyze single-cell behaviors provide a useful tool for next-generation therapeutic development and synthetic biology workflows.

VII. Conclusion and Future Perspectives

Since its inception in 2005, the integration of OET and microfluidics has established a powerful platform for micromanipulation, with profound impacts across biology, chemistry, and biomedical engineering. As this review has systematically detailed, the technology has matured significantly in its principles, applications, and commercialization. Today, the augmentation of these systems with AI is catalyzing a paradigm shift, transforming them from proficient automated tools into intelligent robotic platforms capable of autonomous perception, decision-making, and learning. This synergy is profoundly enhancing manipulation accuracy, throughput, and stability. Looking forward, the continued evolution of this domain will be propelled by a synergistic triad of interconnected frontiers: foundational innovations in chip substrate materials, the deepening of system intelligence towards full autonomy, and the pursuit of disruptive applications in precision medicine.

However, to fully realize this autonomous and precision-driven future, researchers must navigate the physical trade-offs inherent in current system architectures. Throughout this review, we have categorized the integration of OET and microfluidics into three primary modalities based on their fluid transport regimes: continuous-flow microchannels, DMF, and OEW. To provide a clear technological roadmap, Table 2 synthesizes these integration strategies. By benchmarking their governing force balances—ranging from hydrodynamic drag in pressure-driven flows to interfacial tension in droplet manipulation—against key performance metrics, this comparative matrix serves as a fundamental selection guide. It delineates the boundaries between throughput, spatial resolution, and fabrication complexity, thereby assisting researchers in aligning the physical capabilities of the platform with the specific transport requirements of their biochemical assays.

Table 2. Comparative technology roadmap of OET integration strategies.

Integration Strategy	OET-Microchannel	OET-DMF (Digital Microfluidics)	OET-OEW (Optoelectrowetting)	Ref.
Transport Regime	Continuous Flow (Low Re, Pressure-driven)	Discrete Droplet (Electrowetting-on-Dielectric)	Continuous/Discrete Hybrid (Light-actuated wetting)	3,227
Dominant Forces	Hydrodynamic Drag (F_{drag}) vs. ODEP (F_{ODEP})	Electrowetting-on-dielectric (F_{EWOD}) vs. ODEP (F_{ODEP})	Optical electrowetting-on-dielectric (F_{OEWOD}) vs. ODEP (F_{ODEP})	161,231
Throughput	High (10^2 - 10^4 cells/min)	Medium (Parallel droplets, serial content)	Low ~ Medium (Limited by switching speed)	227,231
Spatial Resolution	Single-cell (~1 μm) Limited by flow speed	Droplet-scale (~100 μm) Fine control via internal OET	Droplet-scale (~50 μm) Limited by light pattern edge	161,207
Fabrication Complexity	Moderate (Requires pumps/valves interconnection)	High (Complex electrode addressing + OET layer)	Low (Unpatterned photoconductive sandwich)	104,231
Physical Constraints	Shear stress on cells; Joule heating at high flow rates	Cross-contamination risk; High voltage requirements	Contact angle saturation; Stability of hydrophobic layer	3,143
Ideal Application	Flow cytometry, Cell sorting, Filtration.	Multi-step chemical synthesis, Rare cell sequencing prep.	Programmable droplet routing, Reagent-free mixing.	39,225

1. Future Directions in Substrate Materials and Optoelectronic Integration

The trajectory of OET-microfluidic technology is intrinsically linked to the innovation of its core component: the photoconductive substrate. Historically, the field has been built upon a foundation of well-established inorganic semiconductor technologies. The predominant material choice has been hydrogenated amorphous silicon (a-Si:H), typically deposited on rigid glass or silicon wafers using chemical vapor deposition (CVD). This material has served as a reliable workhorse due to its mature fabrication processes and stable optoelectronic properties. Meanwhile, within the existing a-Si:H system, optimizing the device engineering, such as using pulsed light instead of continuous light to reduce the total heat input, or depositing a transparent

passivation protective layer on the surface of a-Si:H, can also effectively extend the device life and enhance its stability. Other inorganic materials, such as cadmium sulfide (CdS) and gallium arsenide (GaAs), have also been explored for specific applications.

However, a fundamental limitation arises when applying these conventional photoconductive layers in high-conductivity solutions, such as physiological buffers or cell culture media, which are essential for most biomedical applications. A critical challenge for standard OET is its limited efficacy in ion-rich, high-conductivity media, such as physiological buffers and cell culture solutions. This limitation arises from two concurrent physical phenomena that render the device ineffective. Firstly, the formation of a compact electrical double layer at the device surface leads to a "field screening effect," which severely attenuates the electric field gradients required for ODEP manipulation. Secondly, the low impedance of the conductive liquid creates a severe "impedance mismatch" with the photoconductive layer, preventing the efficient coupling of the applied AC potential into the liquid upon illumination. To circumvent this fundamental bottleneck, researchers have developed more sophisticated device architectures, most notably phototransistor-based OETs, designed specifically to operate effectively in these challenging environments. While functionally effective, these devices require multi-layer photolithography and complex fabrication steps, leading to prohibitively high costs and low manufacturing throughput. This inherent trade-off between performance in biological media and fabrication complexity remains the primary barrier to the widespread adoption and commercialization of OET technology.

To overcome this challenge, the research frontier is rapidly shifting towards a new generation of materials that promise high performance without the associated cost and fabrication hurdles. The focus is twofold: enhancing optoelectronic efficiency and diversifying device functionality. To directly replace complex phototransistors, emerging materials like two-dimensional (2D) semiconductors (e.g., MoS_2) and metal-halide perovskites are gaining significant attention[257-260]. These materials offer superior carrier mobility, suppressed dark current, and high quantum yields, enabling the generation of strong ODEP forces even in high-conductivity media but with a much simpler single-layer device structure. Concurrently, to

break free from rigid substrates, research into flexible and biocompatible polymers (e.g., PDMS) is enabling novel form factors for wearable or implantable devices. This progress is further accelerated by advanced fabrication techniques like additive manufacturing (3D printing), which democratize the production of customized microfluidics and reduce the reliance on expensive cleanroom facilities, paving the way for a new ecosystem of low-cost, high-performance, and application-specific OET-microfluidic platforms.

To navigate this evolving material landscape, **Table 3** provides a comparative analysis of these substrates, benchmarking their key physical parameters—ranging from carrier mobility to electrochemical stability—against the boundary conditions imposed by ionic physiological environments.

Table 3. Physical and electrochemical comparison of representative photoconductive materials for OET platforms.

Material	Light/Dark Conductivity Ratio (σ_{light} /σ_{dark})	Photoelectric Response	Stability in Solutions	Fabrication	Applicability & Physical Limitations	Ref.
a-Si:H (Benchmark)	~ 10^3 - 10^4	Moderate mobility; Broad visible absorption	Susceptible to electrochemical oxidation and anodic dissolution	High (Vacuum PECVD required)	Standard choice. Requires protective dielectric layers (e.g., Si_3N_4) which attenuates the effective DEP force.	3,256
2D TMDs (e.g., MoS_2, WSe_2)	~ 10^2 - 10^3	High in-plane mobility; Tunable bandgap (visible to NIR)	Chemically inert via van der Waals surfaces	High (CVD growth and transfer)	Ideal for high-conductivity buffers. Ultra-thin nature minimizes thermal mass, though large-area defect-free scaling remains challenging.	257,260
Halide Perovskites	> 10^4	High mobility; Exceptional absorption	Rapid structural degradation [57]	Low (Solution-processable)	Promising for non-aqueous droplet OEW. Application	258,259

		coefficient	via hydrolysis/ion migration		in standard bio-OET is physically blocked unless heavily passivated. Cost-effective disposable chips.	
Organic Polymers (e.g., TiOPc)	~ 10^2 - 10^3	Low mobility; Exciton-dominated transport	Prone to swelling or degradation over time	Low (Spin-coating/Printing)	Slower switching speeds due to low carrier mobility restrict high-frequency manipulation.	95, 96

2. Intelligent Operating Systems: From AI-Assisted Control to Autonomous Discovery

If material innovation constitutes the "hardware" foundation, then the deep integration of AI represents the "software" core, which will unleash the transformative potential of the OET-microfluidic integrated platform. Before becoming a "phenomenon-level" intelligent laboratory, OET-microfluidic integration technology needs to go through three different but interrelated logical advancements in the intelligent layer: (1) AI-driven object operation optimization, (2) AI-driven interpretation of experimental results, and (3) AI-local design of the physical system itself.

The initial and most mature application of AI in the OET-microfluidics field lies in enhancing the accuracy and efficiency of physical operations, often being applied to the recognition of manipulated targets and navigation within the system, which represents the fundamental layer of system intelligence[261-263]. Currently, deep learning models, especially convolutional neural networks like YOLO[209], have demonstrated outstanding capabilities in real-time, label-free recognition and microscopic target classification (for example, distinguishing different cell types or states). Operating seamlessly atop this perception layer, the actuation and path-planning layer is increasingly governed by Multi-Agent Reinforcement Learning (MARL). Navigating thousands of individual objects in parallel within a dynamically perturbing fluidic environment presents a highly non-linear control problem. Instead of relying

on rigid heuristics, MARL algorithms (such as Deep Q-Networks) train agents in physics-simulated environments to dynamically coordinate collision-less spatiotemporal trajectories. By treating hydrodynamic drag and Brownian stochasticity as environmental variables, these reinforcement learning strategies establish a higher level of robustness and adaptability, enabling the system to instantaneously adjust operational strategies in response to unforeseen fluidic events or unexpected cellular behaviors To systematically contextualize this progression within the physical constraints of micro-scale electrokinetics, it is essential to trace the evolution of these control architectures. Historically, overcoming the stochasticity of Brownian motion and the highly non-linear spatial gradients of the generated force fields relied on manual operation or classical closed-loop algorithms (such as PID or Model Predictive Control)[3,264-267]. However, as manipulation scales up, these traditional methods struggle to dynamically compensate for coupled transport regimes and fluidic inertia. **Table 4** summarizes this technological evolution, benchmarking how each control strategy handles the intrinsic physical non-linearities of the system. This transition from classical error-correction to the physics-informed deep learning frameworks discussed above marks the critical leap toward truly autonomous manipulation.

Table 4. Evolution of control strategies and visual feedback mechanisms in OET manipulation.

Control Strategy / Feedback	Physical Operating Principle	Handling of Non-linear Forces & Fluid Dynamics	Key Advantages	Physical Limitations & Bottlenecks	Ref.
Open-Loop / Manual Control	Human-in-the-loop observation with predefined light pattern actuation	Fails to dynamically compensate for stochastic Brownian motion or sudden flow perturbations.	Simple implementation; suitable for static trapping or low-speed routing.	Extremely low throughput; prone to target loss due to unmodeled hydrodynamic drag.	3,267
Classical Closed-Loop (PID)	Error-based continuous correction using static computer vision	Assumes local linearity. Fails when F_{DEP} gradients change abruptly or when	Effective for steady-state holding and slow, single-target	Struggles with the highly non-linear nature of $\nabla\|\boldsymbol{E}\|$; cannot predict fluidic	263, 266

	thresholds	coupled with varying continuous flow.	trajectory tracking.	inertia.	
Model Predictive Control (MPC)	Receding horizon optimization using explicit physical models of F_{drag} and F_{DEP}	Proactively calculates trajectories by setting physical boundary conditions (e.g., maximum allowable velocity, light intensity limits).	Inherently handles multi-variable physical constraints, preventing cell photothermal damage.	Computationally expensive; relies heavily on the accuracy of the predefined electrokinetic model.	264, 265
Deep Learning & Machine Vision (CNNs, Physics-informed AI)	Data-driven or physics-informed mapping of complex hydrodynamic domains	Decodes dynamic optical contrast and overlapping boundary conditions; predicts non-linear trajectories under flow.	Robust against cellular debris and changing background noise; enables real-time, multi-target pose estimation.	Requires extensive training datasets; "black-box" nature can sometimes obscure the underlying physical transport mechanisms.	234, 261

In the OET-microfluidic integrated system, AI will further play the role of an intelligent analyst. This includes authorizing the system to understand the significance of the experiments it performs. Future platforms will integrate complex AI models and be capable of conducting intelligent analysis of experimental results. For instance, AI will be able to quantify the subtle phenotypic changes in processed cells, identify complex patterns of intercellular interactions, or directly detect the expected results from the imaging data on the chip. This analytical ability is the foundation for achieving robust decentralized diagnostic decisions. In the point-of-care environment, embedded AI can not only provide raw data but also offer direct and reliable diagnostic conclusions, effectively acting as an "expert on the chip", converting complex biological signals into clinically actionable information.

AI is expected to play a significant role in system decision-making to optimize the peak performance of physical systems. The ultimate stage of this evolution is to utilize AI not only as an operator or analyst, but also as a co-designer of the microfluidic system itself. This represents the highest level of integration, in which AI helps the concept of hardware to maximize its performance. By leveraging generative AI and reverse design principles, we can move towards the optimization of AI-driven microfluidic architectures. By providing AI with a set of performance goals (such as "maximizing the purity of cell sorting" or "minimizing reagent consumption"), AI can explore a vast design space and propose novel microchannels that go beyond common intuition.

3. Transformative Applications: A Multi-Scale Vision for Precision Medicine

The ultimate promise of the intelligent OET-microfluidic platform lies in its capacity to revolutionize precision medicine. Rather than merely automating existing protocols, its true disruptive potential is in enabling a seamless, multi-scale analysis of biological systems, progressing logically from the genome to the proteome and culminating at the cellular level. This holistic approach is fundamentally dependent on the previously discussed synergistic advancements in both optoelectronic materials and AI-driven control.At the genomic level, the platform directly addresses the critical challenge of cellular heterogeneity, a primary factor in disease progression and therapeutic resistance. While single-cell sequencing is powerful, its insights are often limited by the purity and viability of the initial input cells. Here, the intelligent OET system functions as an unparalleled front-end sorter. Empowered by AI-driven machine vision, it can perform label-free identification and gentle, high-purity isolation of extremely rare cells (e.g., circulating tumor cells or specific immune subsets) directly from complex clinical samples. This capability is made viable by novel substrate materials that maintain high performance in conductive physiological buffers, ensuring that the isolated cells are in a pristine state for downstream genomic and transcriptomic analysis. The result is a much higher fidelity view of the genetic and transcriptional landscape of disease.

Moving to the proteomic level, the system offers capabilities beyond the static information of a genome. It enables the dynamic functional analysis of individual cells by probing their

protein expression and secretions (the secretome). An AI-controlled OET can isolate a single cell, confine it within a picoliter-scale droplet, and perform on-chip assays to quantify secreted proteins in real-time. This provides a direct measure of cellular function and response to stimuli, such as a candidate drug. Such experiments rely on advanced, biocompatible chip materials that prevent non-specific protein adsorption and sophisticated AI control to precisely manipulate the cell and surrounding reagents, transforming the platform into a high-throughput single-cell functional proteomics engine. The capability of OET to non-destructively manipulate single-cells is critical for such applications.

Finally, at the cellular systems level, the platform culminates as a dynamic micro-environment for orchestrating complex biological processes. It transcends analysis to become a tool for synthesis and intervention. For instance, researchers can use AI to precisely assemble multi-cellular architectures (e.g., an immune synapse between a T-cell and a tumor cell) to investigate cell-cell interactions with unprecedented control. In a therapeutic context, this capability finds its ultimate expression in decentralized cell therapy manufacturing. The entire CAR-T production workflow—from T-cell selection and activation to gene transduction and expansion—can be automated within a closed, desktop-sized OET-microfluidic system. This "cell factory in a box" relies on scalable, low-cost, and disposable chips for clinical use and a highly autonomous AI operating system to monitor and control the entire multi-day process, ensuring the quality and consistency of the final living drug. In essence, the OET-microfluidic platform, powered by the convergence of advanced materials and AI, is evolving into an indispensable multi-scale interrogation tool. It uniquely connects molecular blueprints (genomics) to functional outputs (proteomics) and emergent behaviors (cellular systems), thereby creating a direct, actionable feedback loop for advancing diagnostics, accelerating drug discovery, and personalizing biomedicine.

In conclusion, OET-microfluidic technology is at the epicenter of a developmental nexus fueled by materials science, AI, and biomedicine. The path forward points towards a profound paradigm shift—from static devices to intelligent, autonomous systems, and from laboratory

research to clinically embedded solutions—that has the potential to redefine the frontiers of life science exploration and the practice of medicine.

Acknowledgements

The authors gratefully acknowledge the support from National Key R&D Program of China (Grant No. 2024YFC3406900, 2023YFE0112400), Beijing Municipal Natural Science Foundation (Grant No. 2242018, L246030, 4242060), National Natural Science Foundation of China (Grant No. 62574023), Chonqing Municipal Natural Science Foundation (Grant No. 2024NSCQ-JQX0192, 2024NSCQ-MSX3784, CSTB2024NSCQ-JQX0034), Shenzhen Science and Technology Program (Grant No. KJZD20240903101359020), Open Research Fund of the State Key Laboratory of Optoelectronic Materials and Technologies (Sun Yat-sen University, Grant No. OEMT-2024- KF-03, OEMT-2025-KF-09), Open Research Fund of State Key Laboratory of Digital Medical Engineering (Southeast University, 2025-K07).

Author Contributions

All authors discussed and wrote the manuscript together. All authors reviewed the final version of the manuscript.

Declarations

Conflict of interest

Hainan Xie is the CEO and co-founder of Optoseeker Biotechnology (Shenzhen) Co., Ltd. Wei Xie is the CTO of Optoseeker Biotechnology (Shenzhen) Co., Ltd. Shuailong Zhang is the co-founder of Optoseeker Biotechnology (Shenzhen) Co., Ltd. Other authors declare no competing interests.

References

[1]A. Ashkin and J.M. Dziedzic, "Optical Trapping and Manipulation of Viruses and Bacteria," Science **235**, 1517-1520 (1987).

[2]A. Ashkin, J.M. Dziedzic, and T. Yamane, "Optical Trapping and Manipulation of Single Cells Using Infrared-Laser Beams," Nature **330**, 769-771 (1987).

[3]P.Y. Chiou, A.T. Ohta, and M.C. Wu, "Massively parallel manipulation of single cells and microparticles using optical images," Nature **436**, 370-372 (2005).

[4]J. Rufo, F.Y. Cai, J. Friend, M. Wiklund, and T.J. Huang, "Acoustofluidics for biomedical applications," Nat. Rev. Methods Primers **2**, 30 (2022).

[5]S.J. Yang, Z.H. Tian, Z.Y. Wang, J. Rufo, P. Li, J. Mai, J.P. Xia, H. Bachman, P.H. Huang, M.X. Wu, C.Y. Chen, L.P. Lee, and T.J. Huang, "Harmonic acoustics for dynamic and selective particle manipulation," Nat. Mater. **21**, 540–546 (2022).

[6]A. Ozcelik, J. Rufo, F. Guo, Y.Y. Gu, P. Li, J. Lata, and T.J. Huang, "Acoustic tweezers for the life sciences," Nat. Methods **15**, 1021-1028 (2018).

[7]J.F. Li, C. Shen, T.J. Huang, and S.A. Cummer, "Acoustic tweezer with complex boundary-free trapping and transport channel controlled by shadow waveguides," Sci. Adv. **7**, eabi5502 (2021).

[8]J.F. Sun, Q. Zhao, Z. Mo, J. Chen, H.Y. Guo, and L.J. Zhang, "Self-powered droplet manipulation for full human-droplet interaction in multiple mediums," Nat. Commun. **16**, 2312 (2025).

[9]Y.K. Jin, W.H. Xu, H.H. Zhang, R.R. Li, J. Sun, S.Y. Yang, M.J. Liu, H.Y. Mao, and Z.A.K. Wang, "Electrostatic tweezer for droplet manipulation," PNAS **119**, e2105459119 (2022).

[10]J.L. Yong, X.L. Li, Y.D. Hu, Y.B. Peng, Z.L. Cheng, T.Y. Xu, C.W. Wang, and D. Wu, "Triboelectric 'electrostatic tweezers' for manipulating droplets on lubricated slippery surfaces prepared by femtosecond laser processing," Int. J. Extreme Manuf. **6**, 035002 (2024).

[11]W.H. Xu, Y.K. Jin, W.B. Li, Y.X. Song, S.W. Gao, B.P. Zhang, L.L. Wang, M.M. Cui, X.T. Yan, and Z.K. Wang, "Triboelectric wetting for continuous droplet transport," Sci. Adv. **8**, eade2085 (2022).

[12]R.H. Soon, Z. Yin, M.A. Dogan, N.O. Dogan, M.E. Tiryaki, A.C. Karacakol, A. Aydin, P. Esmaeili-Dokht, and M. Sitti, "Pangolin-inspired untethered magnetic robot for on-demand biomedical heating applications," Nat. Commun. **14**, 3320 (2023).

[13]S.Z. Yi, L. Wang, Z.P. Chen, J. Wang, X.Y. Song, P.F. Liu, Y.X. Zhang, Q.Q. Luo, L.L. Peng, Z.G. Wu, C.A.F. Guo, and L.L. Jiang, "High-throughput fabrication of soft magneto-origami machines," Nat. Commun. **13**, 4177 (2022).

[14]S. Kim, S. Lee, J. Lee, B.J. Nelson, L. Zhang, and H. Choi, "Fabrication and Manipulation of Ciliary Microrobots with Non-reciprocal Magnetic Actuation," Sci. Rep. **6**, 30713 (2016).

[15]N. Xiang, J. Wang, Q. Li, Y. Han, D. Huang, and Z.H. Ni, "Precise Size-Based Cell Separation via the Coupling of Inertial Microfluidics and Deterministic Lateral Displacement," Anal. Chem. **91**, 10328-10334 (2019).

[16]J. Tan, Z. Fan, M.F. Zhou, T. Liu, S.L. Sun, G.J. Chen, Y.C. Song, Z.K. Wang, and D.Y. Jiang, "Orbital Electrowetting-on-Dielectric for Droplet Manipulation on Superhydrophobic Surfaces," Adv. Mater. **36** (2024).

[17]A. S. B, D. C. P, J.C. Chen, and Z.G. Chen, "Optical disassembly of cellular clusters by tunable 'tug-of-war' tweezers," Light Sci. Appl. **5**, e16158-e16158 (2016).

[18]J.L. Killian, F. Ye, and M.D. Wang, "Optical Tweezers: A Force to Be Reckoned With," Cell **175**, 1445-1448 (2018).

[19]R.L. Eriksen, V.R. Daria, and J. Glückstad, "Fully dynamic multiple-beam optical tweezers," Opt. Express **10**, 597-602 (2002).

[20]K. Dholakia, "Micromanipulation - Optoelectronic tweezers," Nat. Mater. **4**, 579-580 (2005).

[21]M.C. Wu, "Optoelectronic tweezers," Nat. Photonics **5**, 322-324 (2011).

[22]K. Wang, E. Schonbrun, P. Steinvurzel, and K.B. Crozier, "Trapping and rotating nanoparticles using a plasmonic nano-tweezer with an integrated heat sink," Nat. Commun. **2**, 469 (2011).

[23]X.L. Peng, Z.H. Chen, P.S. Kollipara, Y.R. Liu, J. Fang, L.H. Lin, and Y.B. Zheng, "Opto-thermoelectric microswimmers," Light Sci. Appl. **9**, 141 (2020).

[24]L.H. Lin, J.L. Zhang, X.L. Peng, Z.L. Wu, A.C.H. Coughlan, Z.M. Mao, M.A. Bevan, and Y.B. Zheng, "Opto-thermophoretic assembly of colloidal matter," Sci. Adv. **3**, e1700458 (2017).

[25]L.H. Lin, X.L. Peng, X.L. Wei, Z.M. Mao, C. Xie, and Y.B. Zheng, "Thermophoretic Tweezers for Low-Power and Versatile Manipulation of Biological Cells," ACS Nano **11**, 3147-3154 (2017).

[26]L. Lin, M. Wang, X. Peng, E.N. Lissek, Z. Mao, L. Scarabelli, E. Adkins, S. Coskun, H.E. Unalan, B.A. Korgel, L.M. Liz-Marzán, E.L. Florin, and Y. Zheng, "Opto-thermoelectric nanotweezers," Nat Photonics **12**, 195-201 (2018).

[27]F.W. Li, J. Wei, X.M. Qin, X. Chen, D.W. Chen, W.T. Zhang, J.G. Han, L.B. Yuan, and H.C. Deng, "Thermo-optical tweezers based on photothermal waveguides," Microsyst. Nanoeng. **10**, 123 (2024).

[28]J.J. Chen, J.X. Zhou, Y.H. Peng, X.Q. Dai, Y. Tan, Y.L. Zhong, T.Z. Li, Y.H. Zou, R. Hu, X.M. Cui, H.P. Ho, B.Z. Gao, H. Zhang, Y. Chen, M.T. Wang, X.J. Zhang, J.L. Qu, and Y.H. Shao, "Highly-Adaptable Optothermal Nanotweezers for Trapping, Sorting, and Assembling across Diverse Nanoparticles," Adv. Mater. **36** (2024).

[29]J. Chen, Z. Chen, C. Meng, J. Zhou, Y. Peng, X. Dai, J. Li, Y. Zhong, X. Chen, W. Yuan, H.-P. Ho, B.Z. Gao, J. Qu, X. Zhang, H. Zhang, and Y. Shao, "CRISPR-powered optothermal nanotweezers: Diverse bio-nanoparticle manipulation and single nucleotide identification," Light Sci. Appl. **12**, 273 (2023).

[30]F. Wang, C. Liu, Z. Dai, W. Xu, X. Ma, Y. Gao, X. Ge, W. Zheng, and X. Du, "Photopyroelectric tweezers for versatile manipulation," Innovation **6**, 100742 (2025).

[31]P.S. Kollipara, X. Li, J. Li, Z. Chen, H. Ding, Y. Kim, S. Huang, Z. Qin, and Y. Zheng, "Hypothermal opto-thermophoretic tweezers," Nat. Commun. **14**, 5133 (2023).

[32]Y. Xie, C. Zhao, Y. Zhao, S. Li, J. Rufo, S. Yang, F. Guo, and T.J. Huang, "Optoacoustic tweezers: a programmable, localized cell concentrator based on opto-thermally generated, acoustically activated, surface bubbles," Lab Chip **13**, 1772-1779 (2013).

[33]Y. Zhang, C. Min, X. Dou, X. Wang, H.P. Urbach, M.G. Somekh, and X. Yuan, "Plasmonic tweezers: for nanoscale optical trapping and beyond," Light Sci. Appl. **10**, 59 (2021).

[34]P. Mestres, J. Berthelot, S.S. Acimovic, and R. Quidant, "Unraveling the optomechanical nature of plasmonic trapping," Light Sci. Appl. **5**, e16092 (2016).

[35]M.L. Juan, M. Righini, and R. Quidant, "Plasmon nano-optical tweezers," Nat. Photonics **5**, 349-356 (2011).

[36]M.-C. Zhong, X.-B. Wei, J.-H. Zhou, Z.-Q. Wang, and Y.-M. Li, "Trapping red blood cells in living animals using optical tweezers," Nat. Commun. **4**, 1768 (2013).

[37]R. Diekmann, D.L. Wolfson, C. Spahn, M. Heilemann, M. Schuettpelz, and T. Huser, "Nanoscopy of bacterial cells immobilized by holographic optical tweezers," Nat. Commun. **7**, 13711 (2016).

[38]T. Wu, T.A. Nieminen, S. Mohanty, J. Miotke, R.L. Meyer, H. Rubinsztein-Dunlop, and M.W. Berns, "A photon-driven micromotor can direct nerve fibre growth," Nat. Photonics **6**, 62-67 (2012).

[39]Z. Guo, F. Li, H. Li, M. Zhao, H. Liu, H. Wang, H. Hu, R. Fu, Y. Lu, S. Hu, H. Xie, H. Ma, and S. Zhang, "Deep Learning-Assisted Label-Free Parallel Cell Sorting with Digital Microfluidics," Adv. Sci. **12** (2025).

[40]E. Liu, C. Wang, H. Zheng, S. Song, A. Riaud, and J. Zhou, "Two-dimensional manipulation of droplets on a single-sided continuous optoelectrowetting digital microfluidic chip," Sensors and Actuators B-Chemical **368**, 132231 (2022).

[41]W.-C. Ho, T.-M. Yu, S.Y. Wei, M.-H. Liu, L. Hsu, and C.-H. Liu, "The Integration of TIOPC-Based Optoelectronic Tweezers and Optoelectrowetting with Frequency Modulation," in Proceedings of the 26th IEEE International

Conference on Micro Electro Mechanical Systems (MEMS), Taipei, TAIWAN, 2013.

[42]S. Zhang, M. Elsayed, R. Peng, Y.J. Chen, Y.F. Zhang, J.X. Peng, W.Z. Li, M.D. Chamberlain, A. Nikitina, S.Y. Yu, X.Y. Liu, S.L. Neale, and A.R. Wheeler, "Reconfigurable multi-component micromachines driven by optoelectronic tweezers," Nat. Commun. **12**, 5349 (2021).

[43]S. Zhang, N. Shakiba, Y. Chen, Y. Zhang, P. Tian, J. Singh, M.D. Chamberlain, M. Satkauskas, A.G. Flood, N.P. Kherani, S. Yu, P.W. Zandstra, and A.R. Wheeler, "Patterned Optoelectronic Tweezers: A New Scheme for Selecting, Moving, and Storing Dielectric Particles and Cells," Small **14**, 1803342 (2018).

[44]W. Yang, H. Yu, G. Li, Y. Wang, and L. Liu, "High-Throughput Fabrication and Modular Assembly of 3D Heterogeneous Microscale Tissues," Small **13**, 1602769 (2017).

[45]C. Witte, J. Reboud, J.M. Cooper, and S.L. Neale, "Channel integrated optoelectronic tweezer chip for microfluidic particle manipulation," J. Micromech. Microeng. **30**, 045004 (2020).

[46]S.K. Thio, S. Bae, and S.-Y. Park, "Plasmonic nanoparticle-enhanced optoelectrowetting (OEW) for effective light-driven droplet manipulation," Sensors and Actuators B-Chemical **308**, 127704 (2020).

[47]E. Liu, C. Wang, L. Du, S. Li, A. Riaud, and J. Zhou, "AI-powered modular and general-purpose droplet processing system based on single-sided continuous optoelectrowetting chip," Sensors and Actuators B-Chemical **420**, 136445 (2024).

[48]A.M. Skelley, O. Kirak, H. Suh, R. Jaenisch, and J. Voldman, "Microfluidic control of cell pairing and fusion," Nat. Methods **6**, 147-152 (2009).

[49]C. Witte, C. Kremer, M. Chanasakulniyom, J. Reboud, R. Wilson, J.M. Cooper, and S.L. Neale, "Spatially Selecting a Single Cell for Lysis Using Light-Induced Electric Fields," Small **10**, 3026-3031 (2014).

[50]L. Zheng, G. Li, H. Du, Z. Li, B. Xu, F. Yang, Y. Mao, J. Wei, H. Xie, W. Xie, R. Fu, N. Liu, S. Zhang, L. Liu, W.J. Li, and Y. Sun, "Automated and collision-free navigation of multiple micro-objects in obstacle-dense microenvironments using optoelectronic tweezers," Microsyst. Nanoeng. **11**, 49 (2025).

[51]Y. Huang, Z.X. Liang, M. Alsoraya, J.H. Guo, and D. Fan, "Light-Gated Manipulation of Micro/Nanoparticles in Electric Fields," Adv. Intell. Syst. **2**, 1900127 (2020).

[52]C.-H. Chuang, Y.-M. Hsu, and C.-C. Yeh, "The effects of nanoparticles uptaken by cells on electrorotation," Electrophoresis **30**, 1449-1456 (2009).

[53]P.-Y. Chiou, A.T. Ohta, A. Jamshidi, H.-Y. Hsu, and M.C. Wu, "Light-actuated ac electroosmosis for nanoparticle manipulation," J. Microelectromech. Syst. **17**, 525-531 (2008).

[54]S. Wang, W. Liang, Z. Dong, V.G.B. Lee, and W.J. Li, "Fabrication of Micrometer- and Nanometer-Scale Polymer Structures by Visible Light Induced Dielectrophoresis (DEP) Force," Micromachines **2**, 431-442 (2011).

[55]N. Liu, P. Li, L. Liu, H. Yu, Y. Wang, G.-B. Lee, and W.J. Li, "3-D Non-UV Digital Printing of Hydrogel Microstructures by Optically Controlled Digital Electropolymerization," J. Microelectromech. Syst. **24**, 2128-2135 (2015).

[56]Y. Li, S.H.S. Lai, N. Liu, G. Zhang, L. Liu, G.-B. Lee, and W.J. Li, "Fabrication of High-Aspect-Ratio 3D Hydrogel Microstructures Using Optically Induced Electrokinetics," Micromachines **7**, 65 (2016).

[57]P. Li, H. Yu, N. Liu, F. Wang, G.-B. Lee, Y. Wang, L. Liu, and W.J. Li, "Visible light induced electropolymerization of suspended hydrogel bioscaffolds in a microfluidic chip," Biomater. Sci. **6**, 1371-1378 (2018).

[58]H.J. Gi, D. Han, and J.-K. Park, "Optoelectrofluidic printing system for fabricating hydrogel sheets with on-demand patterned cells and microparticles," Biofabrication **9**, 015011 (2017).

[59]W. Yang, H. Yu, F. Wei, G. Li, Y. Wang, and L. Liu, "Selective pattern of cancer cell accumulation and growth using UV modulating printing of hydrogels," Biomed. Microdevices **17** (2015).

[60]H. Hwang, H. Chon, J. Choo, and J.-K. Park, "Optoelectrofluidic Sandwich Immunoassays for Detection of Human Tumor Marker Using Surface-Enhanced Raman Scattering," Anal. Chem. **82**, 7603-7610 (2010).

[61]F. Wang, F. Fei, L. Liu, H. Yu, P. Yu, Y. Wang, G.-B. Lee, and W. Jung, "Exploring pulse-voltage-triggered optically induced electrohydrodynamic instability for femtolitre droplet generation," Appl. Phys. Lett. **104**, 264103 (2014).

[62]S. Park, S. Kalim, C. Callahan, M.A. Teitell, and E.P.Y. Chiou, "A light-induced dielectrophoretic droplet manipulation platform," Lab Chip **9**, 3228-3235 (2009).

[63]S. Park, C. Pan, T.-H. Wu, C. Kloss, S. Kalim, C.E. Callahan, M. Teitell, and E.P.Y. Chiou, "Floating electrode optoelectronic tweezers: Light-driven dielectrophoretic droplet manipulation in electrically insulating oil medium," Appl. Phys. Lett. **92**, 151101 (2008).

[64]E. Munoz-Cortes, A. Puerto, A. Blazquez-Castro, L. Arizmendi, J.L. Bella, C. Lopez-Fernandez, M. Carrascosa, and A. Garcia-Cabanes, "Optoelectronic generation of bio-aqueous femto-droplets based on the bulk photovoltaic effect," Opt. Lett. **45**, 1164-1167 (2020).

[65]D.-H. Lee, H. Hwang, and J.-K. Park, "Generation and manipulation of droplets in an optoelectrofluidic device integrated with microfluidic channels," Appl. Phys. Lett. **95**, 164102 (2009).

[66]M. Esseling, A. Zaltron, W. Horn, and C. Denz, "Optofluidic droplet router," Laser Photonics Rev. **9**, 98-104 (2015).

[67]J. Filippi, P. Casti, V. Lacconi, G. Antonelli, M. D'Orazio, G. Curci, C. Ticconi, R. Rago, M. De Luca, A. Pecora, A. Mencattini, S.L. Neale, L. Campagnolo, and E. Martinelli, "ODEP-Based Robotic System for Micromanipulation and In-Flow Analysis of Primary Cells," Cyborg Bionic Syst. **6**, 0234 (2025).

[68]W. Liang, Y. Zhao, L. Liu, Y. Wang, Z. Dong, W.J. Li, G.-B. Lee, X. Xiao, and W. Zhang, "Rapid and Label-Free Separation of Burkitt's Lymphoma Cells from Red Blood Cells by Optically-Induced Electrokinetics," PLoS One **9**, e90827 (2014).

[69]A.H. Jeorrett, S.L. Neale, D. Massoubre, E. Gu, R.K. Henderson, O. Millington, K. Mathieson, and M.D. Dawson, "Optoelectronic tweezers system for single cell manipulation and fluorescence imaging of live immune cells," Opt. Express **22**, 1372-1380 (2014).

[70]S.-B. Huang, J. Chen, J. Wang, C.-L. Yang, and M.-H. Wu, "A New Optically-Induced Dielectrophoretic (ODEP) Force-Based Scheme for Effective Cell Sorting," Int. J. Electrochem. Sci. **7**, 12656-12667 (2012).

[71]H.Y. Hsu, A. Jamshidi, S. Shekarchian, W. Lam, J.K. Valley, S.N. Pei, and M.C. Wu, "Open-Access Phototransistor-Based Optoelectronic Tweezers for Long-Term Single Cell Heterogeneity Study," in Proceedings of the 24th IEEE International Conference on Micro Electro Mechanical Systems (MEMS), Cancun, MEXICO, 2011.

[72]C.Y. Gan, J.Y. Zhang, B. Chen, A. Wang, H.Y. Xiong, J.W. Zhao, C.T. Wang, S.Z. Liang, and L. Feng, "Optoelectronic Tweezers Micro-Well System for Highly Efficient Single-Cell Trapping, Dynamic Sorting, and Retrieval," Small **20** (2024).

[73]Y. Yang, Y. Mao, K.-S. Shin, C.O. Chui, and P.-Y. Chiou, "Self-Locking Optoelectronic Tweezers for Single-Cell and Microparticle Manipulation across a Large Area in High Conductivity Media," Sci. Rep. **6**, 22630 (2016).

[74]C. Vaillier, T. Honegger, F. Kermarrec, X. Gidrol, and D. Peyrade, "Comprehensive Analysis of Human Cells Motion under an Irrotational AC Electric Field in an Electro-Microfluidic Chip," PLoS One **9**, e95231 (2014).

[75]A.T. Ohta, P.-Y. Chiou, H.L. Phan, S.W. Sherwood, J.M. Yang, A.N.K. Lau, H.-Y. Hsu, A. Jamshidi, and M.C. Wu, "Optically controlled cell discrimination and trapping using optoelectronic tweezers," IEEE J. Sel. Top. Quantum Electron. **13**, 235-243 (2007).

[76]L. Miccio, V. Marchesano, M. Mugnano, S. Grilli, and P. Ferraro, "Light induced DEP for immobilizing and orienting Escherichia coli bacteria," Opt. Lasers Eng. **76**, 34-39 (2016).

[77]F. Wang, L. Liu, G. Li, P. Li, Y. Wen, G. Zhang, Y. Wang, G.-B. Lee, and W.J. Li, "Thermo metry of photo sensitive and optically induced electrokinetics chips," Microsyst. Nanoeng. **4**, 26 (2018).

[78]F. Wang, H. Yu, N. Liu, J.D. Mai, L. Liu, G.-B. Lee, and W.J. Li, "Non-ultraviolet-based patterning of polymer structures by optically induced electrohydrodynamic instability," Appl. Phys. Lett. **103**, 214101 (2013).

[79]Y. Liu, C. Wu, H.S.S. Lai, Y.T. Liu, W.J. Li, and Y.J. Shen, "Three-Dimensional Calcium Alginate Hydrogel Assembly via TiOPc-Based Light-Induced Controllable Electrodeposition," Micromachines **8**, 192 (2017).

[80]G. Dai, W. Wan, Y. Zhao, Z. Wang, W. Li, P. Shi, and Y. Shen, "Controllable 3D alginate hydrogel patterning via visible-light induced electrodeposition," Biofabrication **8**, 025004 (2016).

[81]S.L. Neale, C. Witte, and J.M. Cooper, "Portable optoelectronic tweezers (OET), taking optical micromanipulation out of the optics lab," in Proceedings of the European Optical Society Annual Meeting, Aberdeen, UK, 2012.

[82]S. Zhang, W. Li, M. Elsayed, P. Tian, A.W. Clark, A.R. Wheeler, and S.L. Neale, "Size-scaling effects for microparticles and cells manipulated by optoelectronic tweezers," Opt. Lett. **44**, 4171-4174 (2019).

[83]S. Zhang, J. Juvert, J.M. Cooper, and S.L. Neale, "Manipulating and assembling metallic beads with Optoelectronic Tweezers," Sci. Rep. **6**, 32840 (2016).

[84]S. Zhang, Y. Liu, J. Juvert, P. Tian, J.-C. Navarro, J.M. Cooper, and S.L. Neale, "Use of optoelectronic tweezers in manufacturing-accurate solder bead positioning," Appl. Phys. Lett. **109**, 221110 (2016).

[85]H. Hwang and J.-K. Park, "Optoelectrofluidic Manipulation of Nanoparticles and Biomolecules," Adv. OptoElectron. **2011**, 482483 (2011).

[86]H. Hwang and J.-K. Park, "Measurement of Molecular Diffusion Based on Optoelectrofluidic Fluorescence Microscopy," Anal. Chem. **81**, 9163-9167 (2009).

[87]H. Hwang and J.K. Park, "Dynamic Light-Activated Control of Local Chemical Concentration in a Fluid," Anal. Chem. **81**, 5865-5870 (2009).

[88]Y.-H. Lin, C.-M. Chang, and G.-B. Lee, "Manipulation of single DNA molecules by using optically projected images," Opt. Express **17**, 15318-15329 (2009).

[89]H.S. Wasisto, J.D. Prades, J. Gülink, and A. Waag, "Beyond solid-state lighting: Miniaturization, hybrid integration, and applications of GaN nano- and micro-LEDs," Appl. Phys. Rev. **6**, 041315 (2019).

[90]A. Wang, C.Y. Gan, H.C. Han, H.Y. Xiong, J.W. Zhao, C.T. Wang, and L. Feng, "Dynamic Adaptive Imaging System on Optoelectronic Tweezers

Platform," in Proceedings of the IEEE International Conference on Robotics and Automation (ICRA), Yokohama, JAPAN, 2024.

[91]H. Hwang, D. Han, Y.-J. Oh, Y.-K. Cho, K.-H. Jeong, and J.-K. Park, "In situ dynamic measurements of the enhanced SERS signal using an optoelectrofluidic SERS platform," Lab Chip **11**, 2518-2525 (2011).

[92]M.A. Zaman, M. Wu, W. Ren, M.A. Jensen, R.W. Davis, and L. Hesselink, "Spectral tweezers: Single sample spectroscopy using optoelectronic tweezers," Appl. Phys. Lett. **124**, 071104 (2024).

[93]W.-P. Chou, H.-M. Wang, J.-H. Chang, T.-K. Chiu, C.-H. Hsieh, C.-J. Liao, and M.-H. Wu, "The utilization of optically-induced-dielectrophoresis (ODEP)-based virtual cell filters in a microfluidic system for continuous isolation and purification of circulating tumour cells (CTCs) based on their size characteristics," Sensors and Actuators B-Chemical **241**, 245-254 (2017).

[94]S. Zhang, W. Li, M. Elsayed, J. Peng, Y. Chen, Y. Zhang, Y. Zhang, M. Shayegannia, W. Dou, T. Wang, Y. Sun, N.P. Kherani, S.L. Neale, and A.R. Wheeler, "Integrated Assembly and Photopreservation of Topographical Micropatterns," Small **17**, e2103702 (2021).

[95]S.-M. Yang, T.-M. Yu, H.-P. Huang, M.-Y. Ku, L. Hsu, and C.-H. Liu, "Dynamic manipulation and patterning of microparticles and cells by using TiOPc-based optoelectronic dielectrophoresis," Opt. Lett. **35**, 1959-1961 (2010).

[96]S.-M. Yang, T.-M. Yu, H.-P. Huang, M.-Y. Ku, S.-Y. Tseng, C.-L. Tsai, H.-P. Chen, L. Hsu, and C.-H. Liu, "Light-driven manipulation of picobubbles on a titanium oxide phthalocyanine-based optoelectronic chip," Appl. Phys. Lett. **98**, 153512 (2011).

[97]L.-Y. Ke, Z.-K. Kuo, Y.-S. Chen, T.-Y. Yen, M. Dong, H.-W. Tseng, and C.-H. Liu, "Cancer immunotherapy μ-environment LabChip: taking advantage of optoelectronic tweezers," Lab Chip **18**, 106-114 (2018).

[98]W. Wang, Y.-H. Lin, R.-S. Guan, T.-C. Wen, T.-F. Guo, and G.-B. Lee, "Bulk-heterojunction polymers in optically-induced dielectrophoretic devices for the manipulation of microparticles," Opt. Express **17**, 17603-17613 (2009).

[99]W. Wang, Y.-H. Lin, T.-C. Wen, T.-F. Guo, and G.-B. Lee, "Selective manipulation of microparticles using polymer-based optically induced dielectrophoretic devices," Appl. Phys. Lett. **96**, 113302 (2010).

[100]H.A. Eggert, F.Y. Kuhnert, K. Buse, J.R. Adleman, and D. Psaltis, "Trapping of dielectric particles with light-induced space-charge fields," Appl. Phys. Lett. **90**, 241909 (2007).

[101]M. Carrascosa, A. Garcia-Cabanes, M. Jubera, J.B. Ramiro, and F. Agullo-Lopez, "LiNbO3: A photovoltaic substrate for massive parallel manipulation and patterning of nano-objects," Appl. Phys. Rev. **2**, 40605 (2015).

[102]A. Blázquez-Castro, A. García-Cabañes, and M. Carrascosa, "Biological applications of ferroelectric materials," Appl. Phys. Rev. **5**, 041101 (2018).

[103]M. Jubera, I. Elvira, A. García-Cabañes, J.L. Bella, and M. Carrascosa, "Trapping and patterning of biological objects using photovoltaic tweezers," Appl. Phys. Lett. **108**, 023703 (2016).

[104]H.-y. Hsu, A.T. Ohta, P.-Y. Chiou, A. Jamshidi, S.L. Neale, and M.C. Wu, "Phototransistor-based optoelectronic tweezers for dynamic cell manipulation in cell culture media," Lab Chip **10**, 165-172 (2010).

[105]S.L. Neale, A.T. Ohta, H.-Y. Hsu, J.K. Valley, A. Jamshidi, and M.C. Wu, "Force versus position profiles of HeLa cells trapped in phototransistor-based optoelectronic tweezers," in Proceedings of the Conference on Emerging Digital Micromirror Device Based Systems and Applications, San Jose, CA, 2009.

[106]W. Liang, S. Wang, Z. Dong, G.-B. Lee, and W.J. Li, "Optical Spectrum and Electric Field Waveform Dependent Optically-Induced Dielectrophoretic (ODEP) Micro-Manipulation," Micromachines **3**, 492-508 (2012).

[107]J.K. Valley, A. Jamshidi, A.T. Ohta, H.Y. Hsu, and M.C. Wu, "Operational regimes and physics present in optoelectronic tweezers," J. Microelectromech. Syst. **17**, 342-350 (2008).

[108]S. Zhang, Y. Zhai, R. Peng, M. Shayegannia, A.G. Flood, J. Qu, X. Liu, N.P. Kherani, and A.R. Wheeler, "Assembly of Topographical Micropatterns with Optoelectronic Tweezers," Adv. Opt. Mater. **7**, 1900669 (2019).

[109]X. Zhu, H. Yi, and Z. Ni, "Frequency-dependent behaviors of individual microscopic particles in an optically induced dielectrophoresis device," Biomicrofluidics **4**, 013202 (2010).

[110]Y.Y. Jia, S. Miao, A. Wang, C.D. Ni, L. Feng, X.W. Wang, and X. Li, "Non-Contact Dexterous Micromanipulation With Multiple Optoelectronic Robots," IEEE Rob. Autom. Lett. **10**, 4412-4419 (2025).

[111]M.A. Zaman, M. Wu, W. Ren, and L. Hesselink, "Impedance matching in optically induced dielectrophoresis: Effect of medium conductivity on trapping force," Appl. Phys. Lett. **125**, 051108 (2024).

[112]H. Hwang, Y. Oh, J.J. Kim, W. Choi, J.K. Park, S.H. Kim, and J. Jang, "Reduction of nonspecific surface-particle interactions in optoelectronic tweezers," Appl. Phys. Lett. **92**, 024108 (2008).

[113]W.F. Liang, L.Q. Liu, S.H.S. Lai, Y.C. Wang, G.B. Lee, and W.J. Li, "Rapid assembly of gold nanoparticle-based microstructures using optically-induced electrokinetics," Opt. Mater. Express **4**, 2368-2380 (2014).

[114]R. Pethig, "Review Article-Dielectrophoresis: Status of the theory, technology, and applications," Biomicrofluidics **4**, 022811 (2010).

[115]H. Hwang and J.-K. Park, "Optoelectrofluidic platforms for chemistry and biology," Lab Chip **11**, 33-47 (2011).

[116]H. Hwang, J.J. Kim, and J.K. Park, "Experimental investigation of electrostatic particle-particle interactions in optoelectronic tweezers," J. Phys. Chem. B **112**, 9903-9908 (2008).

[117]Z. Tian, X. Wang, and J. Chen, "On-chip dielectrophoretic single-cell manipulation," Microsyst. Nanoeng. **10**, 117 (2024).

[118]Y.-S. Chen, C.P.-K. Lai, C. Chen, and G.-B. Lee, "Isolation and recovery of extracellular vesicles using optically-induced dielectrophoresis on an integrated microfluidic platform," Lab Chip **21**, 1475-1483 (2021).

[119]S.L. Neale, A.T. Ohta, H.-Y. Hsu, J.K. Valley, A. Jamshidi, and M.C. Wu, "Trap profiles of projector based optoelectronic tweezers (OET) with HeLa cells," Opt. Express **17**, 5232-5239 (2009).

[120]J. Yang, Y. Huang, X.B. Wang, F.F. Becker, and P.R.C. Gascoyne, "Cell separation on microfabricated electrodes using dielectrophoretic/gravitational field flow fractionation," Anal. Chem. **71**, 911-918 (1999).

[121]C. Qian, H.B. Huang, L.G. Chen, X.P. Li, Z.B. Ge, T. Chen, Z. Yang, and L.N. Sun, "Dielectrophoresis for Bioparticle Manipulation," Int. J. Mol. Sci. **15**, 18281-18309 (2014).

[122]S. Zhang, A. Nikitina, Y.J. Chen, Y.F. Zhang, L. Liu, A.G. Flood, J. Juvert, M.D. Chamberlain, N.P. Kherani, S.L. Neale, and A.R. Wheeler, "Escape from an optoelectronic tweezer trap: experimental results and simulations," Opt. Express **26**, 5300-5309 (2018).

[123]E. Guzman-Saleh, V.H. Perez-Gonzalez, and R. Martinez-Duarte, "Comparing Different Light Models for Virtual Electrodes in Optoelectronic Tweezers," Electrophoresis **46**, 1333-1340 (2025).

[124]R. Pethig, "Protein Dielectrophoresis: A Tale of Two Clausius-Mossottis-Or Something Else?," Micromachines (Basel) **13** (2022).

[125]S. Kumar and P.J. Hesketh, "Interpretation of ac dielectrophoretic behavior of tin oxide nanobelts using Maxwell stress tensor approach modeling," Sensors and Actuators B-Chemical **161**, 1198-1208 (2012).

[126]X.J. Wang, X.B. Wang, and P.R.C. Gascoyne, "General expressions for dielectrophoretic force and electrorotational torque derived using the Maxwell stress tensor method," J. Electrostat. **39**, 277-295 (1997).

[127]A. Kumar, J.S. Kwon, S.J. Williams, N.G. Green, N.K. Yip, and S.T. Wereley, "Optically Modulated Electrokinetic Manipulation and Concentration of Colloidal Particles near an Electrode Surface," Langmuir **26**, 5262-5272 (2010).

[128]A. Castellanos, A. Ramos, A. González, N.G. Green, and H. Morgan, "Electrohydrodynamics and dielectrophoresis in microsystems:: scaling laws," Journal of Physics D-Applied Physics **36**, 2584-2597, Pii s0022-3727(03)63619-3 (2003).

[129]P.Y. Chiou, A.T. Ohta, A. Jamshidi, H.Y. Hsu, and M.C. Wu, "Light-actuated ac electroosmosis for nanoparticle manipulation," J. Microelectromech. Syst. **17**, 525-531 (2008).

[130]J.W. Zhao, B. Chen, C.Y. Gan, S.X. Huang, H.Y. Xiong, J.W. Ye, P. Zhang, and L. Feng, "Study of particle equilibrium based on the combination of light-actuated AC electroosmosis and light-actuated dielectrophoresis," Opt. Express **32**, 24563-24572 (2024).

[131]A. Mishra, K. Clayton, V. Velasco, S.J. Williams, and S.T. Wereley, "Dynamic optoelectric trapping and deposition of multiwalled carbon nanotubes," Microsyst. Nanoeng. **2**, 16005 (2016).

[132]K.C. Neuman and A. Nagy, "Single-molecule force spectroscopy: optical tweezers, magnetic tweezers and atomic force microscopy," Nat. Methods **5**, 491-505 (2008).

[133]O.M. Maragò, P.H. Jones, P.G. Gucciardi, G. Volpe, and A.C. Ferrari, "Optical trapping and manipulation of nanostructures," Nat. Nanotechnol. **8**, 807-819 (2013).

[134]K.C. Neuman, E.H. Chadd, G.F. Liou, K. Bergman, and S.M. Block, "Characterization of photodamage to Escherichia coli in optical traps," Biophys. J. **77**, 2856-2863 (1999).

[135]X.T. Zhao, Y. Shi, T. Pan, D.Y. Lu, J.Y. Xiong, B.J. Li, and H.B. Xin, "In Situ Single-Cell Surgery and Intracellular Organelle Manipulation Via Thermoplasmonics Combined Optical Trapping," Nano Lett. **22**, 402-410 (2022).

[136]X. Li, S.H. Zhong, T. Pan, J.Y. Xiong, G.S. Zhu, Y. Shi, and H.B. Xin, "Light-powered phagocytic macrophage microrobot (phagobot): both in vitro and in vivo," Light-Science & Applications **14**, 202 (2025).

[137]G.S. Zhu, J.Y. Xiong, X. Li, Z.Y. He, S.H. Zhong, J.L. Chen, Y. Shi, T. Pan, L. Zhang, B.J. Li, and H.B. Xin, "Neural stimulation and modulation with sub-cellular precision by optomechanical bio-dart," Light-Science & Applications **13**, 258 (2024).

[138]H.B. Xin, N. Zhao, Y.N. Wang, X.T. Zhao, T. Pan, Y. Shi, and B.J. Li, "Optically Controlled Living Micromotors for the Manipulation and Disruption of Biological Targets," Nano Lett. **20**, 7177-7185 (2020).

[139]J.Y. Xiong, Z.Y. He, G.S. Zhu, X. Li, Y. Shi, T. Pan, S.H. Zhong, H. Wang, Z.H. Su, L.L. Ye, B.J. Li, and H.B. Xin, "Photonic nanojet-regulated soft microalga-robot with controllable deformation and navigation capability," Photonix **5**, 43 (2024).

[140]Y. Shi, L.R. Liu, J.P. Huang, J.Y. Xiong, S.H. Zhong, G.S. Zhu, X. Li, Z.Y. He, T. Pan, H.B. Xin, and B.J. Li, "Adaptive Opto-Thermal-Hydrodynamic Manipulation and Polymerization (AOTHMAP) for 4D Colloidal Patterning," Adv. Mater. **36**, 2412895 (2024).

[141]J.Y. Xiong, Y. Shi, T. Pan, D.Y. Lu, Z.Y. He, D.N. Wang, X. Li, G.S. Zhu, B.J. Li, and H.B. Xin, "Wake-Riding Effect-Inspired Opto-Hydrodynamic Diatombot for Non-Invasive Trapping and Removal of Nano-Biothreats," Adv. Sci. **10**, 2301365 (2023).

[142]S.L. Leung, Y. Lu, D. Bluestein, and M.J. Slepian, "Dielectrophoresis-Mediated Electrodeformation as a Means of Determining Individual Platelet Stiffness," Ann. Biomed. Eng. **44**, 903-913 (2016).

[143]S. Tada and Y. Seki, "Analysis of Temperature Field in the Dielectrophoresis-Based Microfluidic Cell Separation Device," Fluids **7**, 263 (2022).

[144]M.P. Hughes, "Strategies for dielectrophoretic separation in laboratory-on-a-chip systems," Electrophoresis **23**, 2569-2582 (2002).

[145]P.R.C. Gascoyne and J. Vykoukal, "Particle separation by dielectrophoresis," Electrophoresis **23**, 1973-1983 (2002).

[146]J. Voldman, "Electrical forces for microscale cell manipulation," Annu. Rev. Biomed. Eng. **8**, 425-454 (2006).

[147]Y. Qiu, S. Wei, J. Li, Z. Zhang, L. Gong, and L. He, "High-throughput sorting of nanoparticles with light-patterned dielectrophoresis force," Opt. Express **31**, 41026-41033 (2023).

[148]Z. Mao, P. Li, M. Wu, H. Bachman, N. Mesyngier, X. Guo, S. Liu, F. Costanzo, and T.J. Huang, "Enriching Nanoparticles via Acoustofluidics," ACS Nano **14**, 12256-12256 (2020).

[149]C.-H. Wang, Y.-H. Lee, H.-T. Kuo, W.-F. Liang, W.-J. Li, and G.-B. Lee, "Dielectrophoretically-assisted electroporation using light-activated virtual microelectrodes for multiple DNA transfection," Lab Chip **14**, 592-601 (2014).

[150]T.-K. Chiu, A.C. Chao, W.-P. Chou, C.-J. Liao, H.-M. Wang, J.-H. Chang, P.-H. Chen, and M.-H. Wu, "Optically-induced-dielectrophoresis (ODEP)-based cell manipulation in a microfluidic system for high-purity isolation of integral circulating tumor cell (CTC) clusters based on their size characteristics," Sensors and Actuators B-Chemical **258**, 1161-1173 (2018).

[151]P.-F. Yang, C.-H. Wang, and G.-B. Lee, "Optically-Induced Cell Fusion on Cell Pairing Microstructures," Sci. Rep. **6**, 22036 (2016).

[152]Y.-C. Hsiao, C.-H. Wang, W.-B. Lee, and G.-B. Lee, "Automatic cell fusion via optically-induced dielectrophoresis and optically-induced locally-enhanced electric field on a microfluidic chip," Biomicrofluidics **12**, 034108 (2018).

[153]Y.-C. Hsiao, C.-H. Wang, W.-B. Lee, and G.-B. Lee, "Automatic Cell Fusion Using Optically-induced Dielectrophoresis and Optically-induced Localized Electric Field on a Structure-free Microfluidic Chip," in Proceedings of the 12th IEEE Annual International Conference on Nano/Micro Engineered and Molecular Systems (IEEE-NEMS), Los Angeles, CA, 2017.

[154]P.-Y. Chu, C.-M. Yang, K.-L. Huang, A.-Y. Wu, C.-H. Hsieh, A.C. Chao, and M.-H. Wu, "Development of an Optically Induced Dielectrophoresis (ODEP) Microfluidic System for High-Performance Isolation and Purification of Bacteria," Biosens.-Basel **13**, 952 (2023).

[155]H.-Y. Wang, C.-Y. Chen, P.-Y. Chu, Y.-X. Zhu, C.-H. Hsieh, J.-J. Lu, and M.-H. Wu, "Application of an optically induced dielectrophoresis (ODEP)-based microfluidic system for the detection and isolation of bacteria with heterogeneity of antibiotic susceptibility," Sensors and Actuators B-Chemical **307**, 127540 (2020).

[156]P.-Y. Chu, C.-H. Hsieh, and M.-H. Wu, "The Combination of Immunomagnetic Bead-Based Cell Isolation and Optically Induced Dielectrophoresis (ODEP)-Based Microfluidic Device for the Negative Selection-Based Isolation of Circulating Tumor Cells (CTCs)," Front. Bioeng. Biotechnol. **8**, 921 (2020).

[157]H. Hwang, D.-H. Lee, W. Choi, and J.-K. Park, "Enhanced discrimination of normal oocytes using optically induced pulling-up dielectrophoretic force," Biomicrofluidics **3**, 014103 (2009).

[158]A.T. Ohta, M. Garcia, J.K. Valley, L. Banie, H.-Y. Hsu, A. Jamshidi, S.L. Neale, T. Lue, and M.C. Wu, "Motile and non-motile sperm diagnostic manipulation using optoelectronic tweezers," Lab Chip **10**, 3213-3217 (2010).

[159]H.Y. Hsu, A.T. Ohta, P.Y. Chiou, A. Jamshidi, and M.C. Wu, "Phototransistor-based optoelectronic tweezers for cell manipulation in highly conductive solution," in Proceedings of the 14th International Conference on Solid-State Sensors, Actuators and Microsystems/21st European Conference on Solid-State Transducers, Lyon, FRANCE, 2007.

[160]Y.S. Lu, Y.P. Huang, J.A. Yeh, C. Lee, and Y.H. Chang, "Controllability of non-contact cell manipulation by image dielectrophoresis (iDEP)," Opt. Quantum Electron. **37**, 1385-1395 (2005).

[161]A.T. Ohta, P.-Y. Chiou, T.H. Han, J.C. Liao, U. Bhardwaj, E.R.B. McCabe, F. Yu, R. Sun, and M.C. Wu, "Dynamic cell and microparticle control via optoelectronic tweezers," J. Microelectromech. Syst. **16**, 491-499 (2007).

[162]G.-B. Lee, H.-C. Wu, P.-F. Yang, and J.D. Mai, "Optically induced dielectropheresis sorting with automated medium exchange in an integrated optofluidic device resulting in higher cell viability," Lab Chip **14**, 2837-2843 (2014).

[163]C.-M. Yang, A.-Y. Wu, J.-C. Yu, P.-Y. Chu, C.-H. Hsieh, and M.-H. Wu, "Virtual Filter Membranes in a Microfluidic System for Sorting and Separating Size-Based Micro Polystyrene Beads by Illumination Intensity Design in Optically Induced Dielectrophoresis (ODEP)," Chemosensors **10**, 540 (2022).

[164]W. Choi, S.H. Kim, J. Jang, and J.K. Park, "Lab-on-a-display: a new microparticle manipulation platform using a liquid crystal display (LCD)," Microfluid. Nanofluid. **3**, 217-225 (2007).

[165]P.-Y. Chu, C.-J. Liao, C.-H. Hsieh, H.-M. Wang, W.-P. Chou, P.-H. Chen, and M.-H. Wu, "Utilization of optically induced dielectrophoresis in a microfluidic system for sorting and isolation of cells with varied degree of viability: Demonstration of the sorting and isolation of drug-treated cancer cells with various degrees of anti-cancer drug resistance gene expression," Sensors and Actuators B-Chemical **283**, 621-631 (2019).

[166]T.-K. Chiu, W.-P. Chou, S.-B. Huang, H.-M. Wang, Y.-C. Lin, C.-H. Hsieh, and M.-H. Wu, "Application of optically-induced-dielectrophoresis in microfluidic system for purification of circulating tumour cells for gene expression analysis-Cancer cell line model," Sci. Rep. **6**, 32851 (2016).

[167]C.-J. Liao, C.-H. Hsieh, T.-K. Chiu, Y.-X. Zhu, H.-M. Wang, F.-C. Hung, W.-P. Chou, and M.-H. Wu, "An Optically Induced Dielectrophoresis (ODEP)-Based Microfluidic System for the Isolation of High-Purity CD45neg/EpCAMneg Cells from the Blood Samples of Cancer PatientsDemonstration and Initial Exploration of the Clinical Significance of These Cells," Micromachines **9**, 563 (2018).

[168]S.-B. Huang, M.-H. Wu, Y.-H. Lin, C.-H. Hsieh, C.-L. Yang, H.-C. Lin, C.-P. Tseng, and G.-B. Lee, "High-purity and label-free isolation of circulating tumor cells (CTCs) in a microfluidic platform by using optically-induced-dielectrophoretic (ODEP) force," Lab Chip **13**, 1371-1383 (2013).

[169]S.-M. Yang, T.-M. Yu, M.-H. Liu, L. Hsu, and C.-H. Liu, "Moldless PEGDA-Based Optoelectrofluidic Platform for Microparticle Selection," Adv. OptoElectron. **2011**, 394683 (2011).

[170]Y.-H. Lin, Y.-W. Yang, Y.-D. Chen, S.-S. Wang, Y.-H. Chang, and M.-H. Wu, "The application of an optically switched dielectrophoretic (ODEP) force for the manipulation and assembly of cell-encapsulating alginate microbeads in a microfluidic perfusion cell culture system for bottom-up tissue engineering," Lab Chip **12**, 1164-1173 (2012).

[171]S.H. Hung, Y.H. Lin, and G.B. Lee, "A microfluidic platform for manipulation and separation of oil-in-water emulsion droplets using optically induced dielectrophoresis," J. Micromech. Microeng. **20**, 045026 (2010).

[172]J. Filippi, D. Di Giuseppe, P. Casti, A. Mencattini, G. Antonelli, M. D'Orazio, F. Corsi, D.D. Canosci, L. Ghibelli, C. Witte, C. Di Natale, S.L. Neale, and E. Martinelli, "Exploiting spectral information in Opto-Electronic Tweezers for cell classification and drug response evaluation," Sensors and Actuators B-Chemical **368**, 132200 (2022).

[173]J. Filippi, P. Casti, G. Antonelli, M. Murdocca, A. Mencattini, F. Corsi, M. D'Orazio, A. Pecora, M. De Luca, G. Curci, L. Ghibelli, F. Sangiuolo, S.L. Neale, and E. Martinelli, "Cell Electrokinetic Fingerprint: A Novel Approach

Based on Optically Induced Dielectrophoresis (ODEP) for In-Flow Identification of Single Cells," Small Methods **8** (2024).

[174]R. Fu, B. Xu, F. Yang, G. Li, Z. Li, H. Li, Y. Lu, and S. Zhang, in *Biophotonic Manipulation*, edited by Baojun Li, Yuchao Li, and Hongbao Xin (Springer Nature Singapore, Singapore, 2025), pp. 113-131.

[175]S. Hu, J. Ye, S. Shi, C. Yang, K. Jin, C. Hu, D. Wang, and H. Ma, "Large-Area Electronics-Enabled High-Resolution Digital Microfluidics for Parallel Single-Cell Manipulation," Anal. Chem. **95**, 6905-6914 (2023).

[176]J. Peng, C. Chan, S. Zhang, A.A. Sklavounos, M.E. Olson, E.Y. Scott, Y. Hu, V. Rajesh, B.B. Li, M.D. Chamberlain, S. Zhang, H. Peng, and A.R. Wheeler, "All-in-One digital microfluidics pipeline for proteomic sample preparation and analysis," Chem. Sci. **14**, 2887-2900 (2023).

[177]K.-W. Huang, Y.-C. Wu, J.-A. Lee, and P.-Y. Chiou, "Microfluidic integrated optoelectronic tweezers for single-cell preparation and analysis," Lab Chip **13**, 3721-3727 (2013).

[178]K.-W. Huang, S. Sattar, J.F. Zhong, C.-H. Chou, H.-K. Tsai, and P.-Y. Chiou, "Electrodes for Microfluidic Integrated Optoelectronic Tweezers," Adv. OptoElectron. **2011**, 375451 (2011).

[179]S.H. Huang, L.Y. Hung, and G.B. Lee, "Continuous nucleus extraction by optically-induced cell lysis on a batch-type microfluidic platform," Lab Chip **16**, 1447-1456 (2016).

[180]Y.-H. Lin and G.-B. Lee, "Optically induced flow cytometry for continuous microparticle counting and sorting," Biosensors & Bioelectronics **24**, 572-578 (2008).

[181]W. Liang, N. Liu, Z. Dong, L. Liu, J.D. Mai, G.-B. Lee, and W.J. Li, "Simultaneous separation and concentration of micro- and nano-particles by optically induced electrokinetics," Sensors and Actuators a-Physical **193**, 103-111 (2013).

[182]S. Ota, S. Wang, Y. Wang, X. Yin, and X. Zhang, "Lipid Bilayer-Integrated Optoelectronic Tweezers for Nanoparticle Manipulations," Nano Lett. **13**, 2766-2770 (2013).

[183]P. Li, N. Liu, H. Yu, F. Wang, L. Liu, G.-B. Lee, Y. Wang, and W.J. Li, "Silver nanostructures synthesis via optically induced electrochemical deposition," Sci. Rep. **6**, 28035 (2016).

[184]M.B. Lim, R.G. Felsted, X. Zhou, B.E. Smith, and P.J. Pauzauskie, "Patterning of graphene oxide with optoelectronic tweezers," Appl. Phys. Lett. **113**, 031106 (2018).

[185]J.-L. Hong, C.-M. Yang, P.-Y. Chu, W.-P. Chou, C.-J. Liao, C.-H. Hsieh, M.-H. Wu, and P.-H. Chen, "The effect of operating conditions on the optically induced electrokinetic (OEK)-based manipulation of magnetic microbeads in a microfluidic system," Sensors and Actuators B-Chemical **296**, 126610 (2019).

[186]S.-M. Yang, P.T. Harishchandra, T.-M. Yu, M.-H. Liu, L. Hsu, and C.-H. Liu, "Concentration of Magnetic Beads Utilizing Light-Induced Electro-Osmosis Flow," IEEE Trans. Magn. **47**, 2418-2421 (2011).

[187]S.J. Lin, S.H. Hung, J.Y. Jeng, T.F. Guo, and G.B. Lee, "Manipulation of micro-particles by flexible polymer-based optically-induced dielectrophoretic devices," Opt. Express **20**, 583-592 (2012).

[188]X.L. Zhu, H. Yi, and Z.H. Ni, "Frequency-dependent behaviors of individual microscopic particles in an optically induced dielectrophoresis device," Biomicrofluidics **4**, 013202 (2010).

[189]Y.C. Tsai, Y.H. Hong, S.J. Zhang, and J.N. Kuo, "Frequency-selective electrokinetic manipulation of microparticles in gold nanofilm optically-induced dielectrophoretic device," Microsystem Technologies-Micro-and Nanosystems-Information Storage and Processing Systems **26**, 1213-1222 (2020).

[190]J.Y. Xiong, X. Li, Z.Y. He, Y. Shi, T. Pan, G.S. Zhu, D.Y. Lu, and H.B. Xin, "Light-controlled soft bio-microrobot," Light-Science & Applications **13**, 55 (2024).

[191]S. Zhang, Y. Liu, Y. Qian, W. Li, J. Juvert, P. Tian, J.-C. Navarro, A.W. Clark, E. Gu, M.D. Dawson, J.M. Cooper, and S.L. Neale, "Manufacturing with light - micro-assembly of opto-electronic microstructures," Opt. Express **25**, 28838-28850 (2017).

[192]S. Zhang, E.Y. Scott, J. Singh, Y. Chen, Y. Zhang, M. Elsayed, M.D. Chamberlain, N. Shakiba, K. Adams, S. Yu, C.M. Morshead, P.W. Zandstra, and A.R. Wheeler, "The optoelectronic microrobot: A versatile toolbox for micromanipulation," PNAS **116**, 14823-14828 (2019).

[193]G. Li, B. Xu, X. Wang, J. Yu, Y. Zhang, R. Fu, F. Yang, H. Gu, Y. Huang, Y. Chen, Y. Zhang, Z. Wang, G. Shen, Y. Wang, H. Xie, A.R. Wheeler, J. Li, and S. Zhang, "Crossing the Dimensional Divide with Optoelectronic Tweezers: Multicomponent Light-Driven Micromachines with Motion Transfer in Three Dimensions," Adv. Mater. **37** (2025).

[194]K. Zhao, G. Chen, R. Fan, Z. Wang, L. Ma, Y. Huo, J. Chen, Y. Zhang, and K. Zhang, "Optically-induced dielectrophoresis: A versatile platform for advanced micromanipulation, precision separation, and integrated device assembly," TrAC, Trends Anal. Chem. **198**, 118760 (2026).

[195]R.F. Wenbo Dong. Bingrui Xu, S.l Fan Yang. Han Cui, Zipeng Zhao. Yifan Zhang. Hang Li..S.Il Kangfu Chen,ll,O xiaorong Hong,Jiangjiang Zhang,Xuekai Liu, Jiafang Li,Yeliang Wang,O Huikai Xielland Shuailong Zhang, "Light-Programmable Nanograspers for Rapid Nanoplastics Detection in Biological Fluids," ACS Nano (2026) doi.org/10.1021/acsnano.5c20989.

[196]E.O. Adekanmbi and S.K. Srivastava, "Dielectric characterization of bioparticles via electrokinetics: The past, present, and the future," Appl. Phys. Rev. **6**, 041313 (2019).

[197]S. Movahed and D. Li, "Microfluidics cell electroporation," Microfluid. Nanofluid. **10**, 703-734 (2011).

[198]L. Chang, L. Li, J. Shi, Y. Sheng, W. Lu, D. Gallego-Perez, and L.J. Lee, "Micro-/nanoscale electroporation," Lab Chip **16**, 4047-4062 (2016).

[199]J.K. Valley, A.T. Ohta, H.-Y. Hsu, S.L. Neale, A. Jamshidi, and M.C. Wu, "Optoelectronic Tweezers as a Tool for Parallel Single-Cell Manipulation and Stimulation," IEEE Trans. Biomed. Circuits Syst. **3**, 424-431 (2009).

[200]J.K. Valley, S. Neale, H.-Y. Hsu, A.T. Ohta, A. Jamshidi, and M.C. Wu, "Parallel single-cell light-induced electroporation and dielectrophoretic manipulation," Lab Chip **9**, 1714-1720 (2009).

[201]C. Kremer, C. Witte, S.L. Neale, J. Reboud, M.P. Barrett, and J.M. Cooper, "Shape-Dependent Optoelectronic Cell Lysis," Angewandte Chemie-International Edition **53**, 842-846 (2014).

[202]Y.-H. Lin and G.-B. Lee, "An optically induced cell lysis device using dielectrophoresis," Appl. Phys. Lett. **94**, 033901 (2009).

[203]C. Witte, C. Kremer, J.M. Cooper, and S.L. Neale, "Continuous cell lysis in microfluidics through acoustic and optoelectronic tweezers," in Proceedings of the Conference on Microfluidics, BioMEMS, and Medical Microsystems XI, San Francisco, CA, 2013.

[204]N. Rondot, S. Yan, D. Mager, and L. Kulinsky, "A low-cost printed circuit board-based centrifugal microfluidic platform for dielectrophoresis," Microsyst. Nanoeng. **11**, 23 (2025).

[205]Z. Jia, C. Chang, S. Hu, J. Li, M. Ge, W. Dong, and H. Ma, "Artificial intelligence-enabled multipurpose smart detection in active-matrix electrowetting-on-dielectric digital microfluidics," Microsystems & Nanoengineering **10**, 139 (2024).

[206]A.H.C. Ng, B.B. Li, M.D. Chamberlain, and A.R. Wheeler, in *Annual Review of Biomedical Engineering, Vol 17*, edited by M. L. Yarmush (2015), Vol. 17, pp. 91-112.

[207]G.J. Shah, A.T. Ohta, E.P. Chiou, M.C. Wu, and C.J. Kim, "EWOD-driven droplet microfluidic device integrated with optoelectronic tweezers as an automated platform for cellular isolation and analysis," Lab Chip **9**, 1732-1739 (2009).

[208]G.J. Shah, P.Y. Chiou, J. Gong, O. Aaron, J.B. Cho, M.C. Wu, C.J. Kim, and H. Natl Inst, "Integrating optoelectronic tweezers for individual particle manipulation with digital microfluidics using electrowetting-on-dielectric (EWOD)," in Proceedings of the 19th IEEE International Conference on Micro Electro Mechanical Systems (MEMS 2006), Istanbul, TURKEY, 2006.

[209]L. Howell, V. Anagnostidis, and F. Gielen, "Multi-Object Detector YOLOv4-Tiny Enables High-Throughput Combinatorial and Spatially-Resolved Sorting of Cells in Microdroplets," Adv. Mater. Technol. **7**, 2101053 (2022).

[210]C. Hong, S. Yang, and J.C. Ndukaife, "Exosomes trapping, manipulation and size-based separation using opto-thermo-electrohydrodynamic tweezers," Nanoscale Adv. **5**, 2973-2978 (2023).

[211]W.-J. Soong, C.-H. Wang, Y.-S. Chen, C. Chen, and G.-B. Lee, "Sorting of Extracellular Vesicles by Using Optically-Induced Dielectrophoresis on an Integrated Microfluidic Chip," in Proceedings of the 36th IEEE International Conference on Micro Electro Mechanical Systems (MEMS), Munich, GERMANY, 2023.

[212]D. Wang, S. Yang, N. Wang, H. Guo, S. Feng, Y. Luo, and J. Zhao, "A Novel Microfluidic Strategy for Efficient Exosome Separation via Thermally Oxidized Non-Uniform Deterministic Lateral Displacement (DLD) Arrays and Dielectrophoresis (DEP) Synergy," Biosens.-Basel **14**, 174 (2024).

[213]M. Lan and F. Yang, "Applications of dielectrophoresis in microfluidic-based exosome separation and detection," Chem. Eng. J. **491**, 152067 (2024).

[214]C.B. Eaker and M.D. Dickey, "Liquid metal actuation by electrical control of interfacial tension," Appl. Phys. Rev. **3**, 031103 (2016).

[215]S. Arscott, "Moving liquids with light: Photoelectrowetting on semiconductors," Sci. Rep. **1**, 184 (2011).

[216]C. Palma and R.D. Deegan, "Droplet Translation Actuated by Photoelectrowetting," Langmuir **34**, 3177-3185 (2018).

[217]F. Krogmann, H. Qu, W. Moench, and H. Zappe, "Push/pull actuation using opto-electrowetting," Sensors and Actuators a-Physical **141**, 499-505 (2008).

[218]P.Y. Chiou, H. Moon, H. Toshiyoshi, C.J. Kim, and M.C. Wu, "Light actuation of liquid by optoelectrowetting," Sensors and Actuators a-Physical **104**, 222-228 (2003).

[219]P.-Y. Chiou, Z. Chang, and M.C. Wu, "Droplet manipulation with light on optoelectrowetting device," J. Microelectromech. Syst. **17**, 133-138 (2008).

[220]D. Jiang and S.-Y. Park, "Light-driven 3D droplet manipulation on flexible optoelectrowetting devices fabricated by a simple spin-coating method," Lab Chip **16**, 1831-1839 (2016).

[221]J.K. Valley, N. Shao, A. Jamshidi, H.-Y. Hsu, and M.C. Wu, "A unified platform for optoelectrowetting and optoelectronic tweezers," Lab Chip **11**, 1292-1297 (2011).

[222]F. Mugele and J.C. Baret, "Electrowetting: From basics to applications," Journal of Physics-Condensed Matter **17**, R705-R774 (2005).

[223]V. Narasimhan and S.-Y. Park, "An Ion Gel as a Low-Cost, Spin-Coatable, High-Capacitance Dielectric for Electrowetting-on-Dielectric (EWOD)," Langmuir **31**, 8512-8518 (2015).

[224]S.K. Thio and S.-Y. Park, "A review of optoelectrowetting (OEW): from fundamentals to lab-on-a-smartphone (LOS) applications to environmental sensors," Lab Chip **22**, 3987-4006 (2022).

[225]S.N. Pei, J.K. Valley, S.L. Neale, H.-Y. Hsu, A. Jamshidi, and M.C. Wu, "Rapid Droplet Mixing Using Light-Actuated Digital Microfluidics," in Proceedings of the Conference on Lasers and Electro-Optics (CLEO)/Quantum Electronics and Laser Science Conference (QELS), San Jose, CA, 2010.

[226]P.Y. Chiou, S.-Y. Park, and M.C. Wu, "Continuous optoelectrowetting for picoliter droplet manipulation," Appl. Phys. Lett. **93**, 221110 (2008).

[227]S.N. Pei, J.K. Valley, S.L. Neale, A. Jamshidi, H.-Y. Hsu, and M.C. Wu, "Light-Actuated Digital Microfluidics for Large-Scale, Parallel Manipulation of Arbitrarily Sized Droplets," in Proceedings of the 23rd IEEE International Conference on Micro Electro Mechanical Systems (MEMS 2010), Hong Kong, PEOPLES R CHINA, 2010.

[228]A. Kumar, H.-S. Chuang, and S.T. Wereley, "Dynamic Manipulation by Light and Electric Fields: Micrometer Particles to Microliter Droplets," Langmuir **26**, 7656-7660 (2010).

[229]H.-S. Chuang, A. Kumar, and S.T. Wereley, "Open optoelectrowetting droplet actuation," Appl. Phys. Lett. **93**, 064104 (2008).

[230]J.T.-A. Loo, *Co-Planar Optoelectrowetting (OEW) Device for Droplet Manipulation*. (2020).

[231]S.-Y. Park, M.A. Teitell, and E.P.Y. Chiou, "Single-sided continuous optoelectrowetting (SCOEW) for droplet manipulation with light patterns," Lab Chip **10**, 1655-1661 (2010).

[232]S.K. Fan, P.W. Huang, T.T. Wang, and Y.H. Peng, "Cross-scale electric manipulations of cells and droplets by frequency-modulated dielectrophoresis and electrowetting," Lab Chip **8**, 1325-1331 (2008).

[233]V.N. Luk, G.C.H. Mo, and A.R. Wheeler, "Pluronic additives: A solution to sticky problems in digital microfluidics," Langmuir **24**, 6382-6389 (2008).

[234]T. Wang, S. Zhou, X. Liu, J. Zeng, X. He, Z. Yu, Z. Liu, X. Liu, J. Jin, Y. Zhu, L. Shi, H. Yan, and T. Zhou, "Intelligent optoelectrowetting digital microfluidic system for real-time selective parallel manipulation of biological droplet arrays," Lab Chip **25** (2025).

[235]T.J. Puchtler et al., "Single-molecule DNA sequencing of widely varying GC-content using nucleotide release, capture and detection in microdroplets," Nucleic Acids Res. **48**, e132 (2020).

[236]L.G. Welch, J. Estranero, P. Tourlomousis, R.C.R. Wootton, V. Radu, C. Gonzalez-Fernandez, T.J. Puchtler, C.M. Murzeau, N.M.G. Dieckmann, A. Shibahara, B.W. Longbottom, C.E. Bryant, and E.L. Talbot, "A programmable and automated optical electrowetting-on-dielectric (oEWOD) driven platform for massively parallel and sequential processing of single cell assay operations," Lab Chip **24** (2024).

[237]S.K. Thio and S.-Y. Park, "Aluminium Nanoparticle-Enhanced Optoelectrowetting Device for Effective Light-Driven Droplet Manipulation,"

in Proceedings of the 32nd IEEE International Conference on Micro Electro Mechanical Systems (IEEE MEMS), Seoul, SOUTH KOREA, 2019.

[238]J. Strassner, C. Doering, E. Oliveira, and H. Fouckhardt, "Optoelectrowetting (OEW) with push-actuation of microdroplets at small frequencies and OEW equations revisited," Sensors and Actuators a-Physical **334**, 113331 (2022).

[239]S.K. Thio, S.W. Bae, and S.-Y. Park, "Lab on a smartphone (LOS): A smartphone-integrated, plasmonic-enhanced optoelectrowetting (OEW) platform for on-chip water quality monitoring through LAMP assays," Sensors and Actuators B-Chemical **358**, 131543 (2022).

[240]Z. Jia, C. Chang, S. Hu, J. Li, M. Ge, W. Dong, and H. Ma, "Artificial intelligence-enabled multipurpose smart detection in active-matrix electrowetting-on-dielectric digital microfluidics," Microsyst Nanoeng **10**, 139 (2024).

[241]D. Jiang, S. Lee, S.W. Bae, and S.-Y. Park, "Smartphone integrated optoelectrowetting (SiOEW) for on-chip sample processing and microscopic detection of water quality," Lab Chip **18**, 532-539 (2018).

[242]L. Nan, H.D. Zhang, D.A. Weitz, and H.C. Shum, "Development and future of droplet microfluidics," Lab Chip **24** (2024).

[243]Z.H. Yu, W.Q. Tong, J.M. Shi, S.Y. Chen, L.L. Shui, H.Y. Chen, L.Y. Shi, J. Jin, and Y.G. Zhu, "Droplet Impedance Feedback-Enabled Microsampling Microfluidic Device for Precise Chemical Information Monitoring," Anal. Chem. **96**, 16946-16954 (2024).

[244]https://www.optoseeker.com/

[245]B. Xu, G. Li, L. Zheng, W. Dong, P. Song, Z. Guo, Z. Li, H. Liu, Z. Ma, H. Xie, W. Xie, H. Li, R. Fu, Y. Lu, N. Liu, H. Xie, and S. Zhang, "Optimizing light pattern curvature to improve the performance of optoelectronic tweezers in micromanipulation," Opt. Express **33**, 2968-2979 (2025).

[246]https://www.berkeleylights.com/

[247]K. Le, C. Tan, H. Le, J. Tat, E. Zasadzinska, J. Diep, R. Zastrow, C. Chen, and J. Stevens, "Assuring Clonality on the Beacon Digital Cell Line Development Platform," Biotechnol. J. **15**, 1900247 (2020).

[248]https://www.berkeleylights.com/blog/racing-to-find-the-rightcells-our-covid-19-success-stories/

[249]M.C. Wu, "Optoelectronic Tweezers-An Optofluidic Platform for Digital Cell Biology," in Proceedings of the International Conference on Optical MEMS and Nanophotonics (OMN), KAIST, Daejeon, SOUTH KOREA, 2019.

[250]A. Winters, K. McFadden, J. Bergen, J. Landas, K.A. Berry, A. Gonzalez, H. Salimi-Moosavi, C.M. Murawsky, P. Tagari, and C.T. King, "Rapid single B cell antibody discovery using nanopens and structured light," Mabs **11**, 1025-1035 (2019).

[251]M. Jorgolli, T. Nevill, A. Winters, I. Chen, S. Chong, F.-F. Lin, M. Mock, C. Chen, K. Le, C. Tan, P. Jess, H. Xu, A. Hamburger, J. Stevens, T. Munro, M. Wu, P. Tagari, and L.P. Miranda, "Nanoscale integration of single cell biologics discovery processes using optofluidic manipulation and monitoring," Biotechnol. Bioeng. **116**, 2393-2411 (2019).

[252]K. Le, C. Tan, S. Gupta, T. Guhan, H. Barkhordarian, J. Lull, J. Stevens, and T. Munro, "A novel mammalian cell line development platform utilizing nanofluidics and optoelectro positioning technology," Biotechnol. Progr. **34**, 1438-1446 (2018).

[253]Y. Bronevetsky, "Directly test individual T cell function with fewer cells on the berkeley lights lightning™ platform," Cytotherapy **22**, S119-S119 (2020).

[254]A. Mocciaro, T.L. Roth, H.M. Bennett, M. Soumillon, A. Shah, J. Hiatt, K. Chapman, A. Marson, and G. Lavieu, "Light-activated cell identification and sorting (LACIS) for selection of edited clones on a nanofluidic device," Commun. Biol. **1**, 41 (2018).

[255]C.W. Shields, C.D. Reyes, and G.P. López, "Microfluidic cell sorting: a review of the advances in the separation of cells from debulking to rare cell isolation," Lab Chip **15**, 1230-1249 (2015).

[256]S.L. Zhang, B.R. Xu, M. Elsayed, F. Nan, W.F. Liang, J.K. Valley, L.Q. Liu, Q. Huang, M.C. Wu, and A.R. Wheeler, "Optoelectronic tweezers: a versatile toolbox for nano-/micro-manipulation," Chem. Soc. Rev. **51**, 9203-9242 (2022).

[257]K.F. Mak, C. Lee, J. Hone, J. Shan, and T.F. Heinz, "Atomically Thin MoS2: A New Direct-Gap Semiconductor," Phys. Rev. Lett. **105**, 136805 (2010).

[258]Z.J. Tan, Y. Wu, H. Hong, J.B. Yin, J.C. Zhang, L. Lin, M.Z. Wang, X. Sun, L.Z. Sun, Y.C. Huang, K.H. Liu, Z.F. Liu, and H.L. Peng, "Two-Dimensional (C4H9NH3)2PbBr4 Perovskite Crystals for High-Performance Photodetector," J. Am. Chem. Soc. **138**, 16612-16615 (2016).

[259]W. Hu, W. Huang, S.Z. Yang, X. Wang, Z.Y. Jiang, X.L. Zhu, H. Zhou, H.J. Liu, Q.L. Zhang, X.J. Zhuang, J.L. Yang, D.H. Kim, and A.L. Pan, "High-Performance Flexible Photodetectors based on High-Quality Perovskite Thin Films by a Vapor-Solution Method," Adv. Mater. **29**, 1703256 (2017).

[260]J. Qin, H. Yan, G. Qiu, M. Si, P. Miao, Y. Duan, W. Shao, L. Zhen, C. Xu, and P.D.J.N.R. Ye, "Hybrid dual-channel phototransistor based on 1D t-Se and 2D ReS2 mixed-dimensional heterostructures," **12**, 669-674 (2019).

[261]J. Zhao, C. Gan, J. Zhang, S. Liang, J. Yang, and L. Feng, "Deep Learning Assisted Automated Separation Platform of Single Cells and Microparticles Using Optoelectronic Tweezers," in Proceedings of the 4th World Robot Conference (WRC) / Symposium on Advanced Robotics and Automation (SARA), Beijing, PEOPLES R CHINA, 2022.

[262]J. Liu, H. Wang, M. Liu, R. Zhao, Y. Zhao, T. Sun, and Q. Shi, "POMDP-Based Real-Time Path Planning for Manipulation of Multiple Microparticles via Optoelectronic Tweezers," Cyborg Bionic Syst. **2022**, 9890607 (2022).

[263]L. Mennillo, C. Bendkowski, M. Elsayed, H. Edwards, S. Zhang, V. Pawar, A.R. Wheeler, D. Stoyanov, and M. Shaw, "Adaptive Autonomous Navigation of Multiple Optoelectronic Microrobots in Dynamic Environments," IEEE Rob. Autom. Lett. **7**, 11102-11109 (2022).

[264]T.Y. Wang, S.Z. Zhou, J.H. Zeng, G.B. Qian, Z.H. Wu, J.M. Bai, L. Sun, Z.H. Yu, H. Yan, T. Zhou, H.M. Chen, and L.Y. Shi, "Artificial potential field-enhanced optoelectronic tweezer technology for path planning and intelligent sorting of particles," Physics of Fluids **37**, 113306 (2025).

[265]E. Erben, I. Saraev, W. Liao, F. Nan, E. Lauga, and M. Kreysing, "Optical Micromanipulations Based on Model Predictive Control of Thermoviscous Flows," Small **21**, e01039 (2025).

[266]D.B. Phillips, "Applications of closed-loop feedback control with holographic optical tweezers," Doctoral dissertation, University of Bristol (2012).

[267]L.H.S. Sam, W.F. Liang, L.Q. Liu, Y.C. Wang, N. Xi, W.J. Li, "Development of a Joystick-controlled Optically-induced Dielectrophoresis Platform for Real-time Micromanipulation," Proceedings of the 2013 IEEE International Conference on Robotics and Biomimetics (ROBIO) (pp. 2749-2754). IEEE.